land

MDPI

Article

A Scientific Investigation of the Shangfang Mountain Yunshui Cave in Beijing Based on LiDAR Technology

Xinyue Liu [1], Yanhui Shan [1], Gang Ai [1,*], Zhengfeng Du [2,*], Anran Shen [1] and Ningfei Lei [1]

[1] School of Information Engineering, China University of Geosciences (Beijing), Haidian, Beijing 100083, China; 1004215211@email.cugb.edu.cn (X.L.); 1004215209@email.cugb.edu.cn (Y.S.); 1004215202@email.cugb.edu.cn (A.S.); 1004215215@email.cugb.edu.cn (N.L.)
[2] Beijing Municipal Commission of Planning and Natural Resources, Changping, Beijing 102200, China
* Correspondence: aigang@cugb.edu.cn (G.A.); cpfjdzf@ghzrzyw.beijing.gov.cn (Z.D.)

Abstract: The Yunshui Cave in Shangfang Mountain, Beijing, is a famous high-altitude karst cave in northern China. As the third scientific survey of Yunshui Cave in history, this is the first time to use the latest LiDAR technology to carry out a related detection survey. Traditional cave measurement methods are limited by natural conditions and make it difficult to reach the destination. Traditional methods mainly rely on experience and obtain data with strong subjectivity, making it difficult to conduct quantitative research and obtain reproducible results in the current information era. Applying LiDAR technology to cave measurement can obtain comprehensive and accurate digital measurement results within the same survey time and reveal many richer and more accurate features of Yunshui Cave. The obtained digital measurement results can be used for 3D modeling as well as provide a large amount of accurate basic data and preliminary materials for subsequent geological, environmental, and archaeological investigation and analysis, as well as cultural and tourism resource development. The rapid geological survey of Shangfang Mountain Yunshui Cave using LiDAR technology shows that LiDAR cave geological survey technology can achieve real-time collection of centimeter-level accuracy and generate billions of points of cloud data, greatly improving survey efficiency and accuracy. At the same time, digital survey results can be obtained. Through modeling and GIS technology, all on-site survey details can be easily moved back to the laboratory for real-scene reproduction, network sharing, and dissemination. This study provides a foundation for future explorations of the Yunshui cave and highlights the potential for LiDAR techniques to enhance our understanding of complex geological structures such as caves.

Keywords: LiDAR (light detection and ranging); karst cave; GIS; surveying and mapping; geologic survey

Citation: Liu, X.; Shan, Y.; Ai, G.; Du, Z.; Shen, A.; Lei, N. A Scientific Investigation of the Shangfang Mountain Yunshui Cave in Beijing Based on LiDAR Technology. *Land* **2024**, *13*, 895. https://doi.org/10.3390/land13060895

Academic Editors: Kenan Li, Xuan Liu and Wenfeng Zheng

Received: 29 May 2024
Revised: 12 June 2024
Accepted: 18 June 2024
Published: 20 June 2024

1. Introduction

Yunshui Cave has a history of more than 2000 years of human activity, which makes it a veritable historical and cultural cave, and it is also the earliest open karst cave in North China. This scientific survey adopted the latest LiDAR technology and conducted precise 3D modeling and multi-dimensional measurement analysis research on the Yunshui Cave in Shangfang Mountain, Beijing. On the one hand, traditional cave survey and measurement methods, such as the previous scientific investigation of Yunshui Cave, used measuring ropes, which not only took time and effort but also affected the accuracy of measurement results due to insufficient light and low visibility inside the cave. Traditional methods mainly rely on experience, resulting in highly subjective data and inaccurate measurement results. The use of laser scanning in our survey reduces working time, and, unlike digital photogrammetry, laser scanning is independent of light [1], so accurate and objective data can be obtained. On the other hand, traditional methods are often limited to two-dimensional mapping [2], and it is difficult to capture the complete three-dimensional

structure of the cave. LiDAR technology can not only quickly obtain comprehensive and accurate digital results but also generate centimeter-level, fully digital 3D models of Yunshui Cave through modeling and share digital results with other researchers for remote collaborative research. LiDAR technology has achieved multiple research results and experiences in the field of new geological survey techniques, aiming to record the study area with high resolution and model the study area to restore the shape of the entire space. This new technology can provide new research methods for the structure and morphology of underground caves [3,4], and it can also assist in archaeological research and the protection of archaeological sites [5,6].

1.1. Shangfang Mountain Yunshui Cave Background Introduction

Yunshui Cave is located on the southern slope of Shangfang Mountain in Fangshan District, Beijing, as shown in Figure 1. The Shangfang Mountain of Beijing belongs to the Great Fangshan branch of Taihang Mountain, which is located in the transition from the western mountainous area of Beijing to the plain [7]. The highest altitude is 864 m, and the slope of the mountain is between 20 and 70 degrees.

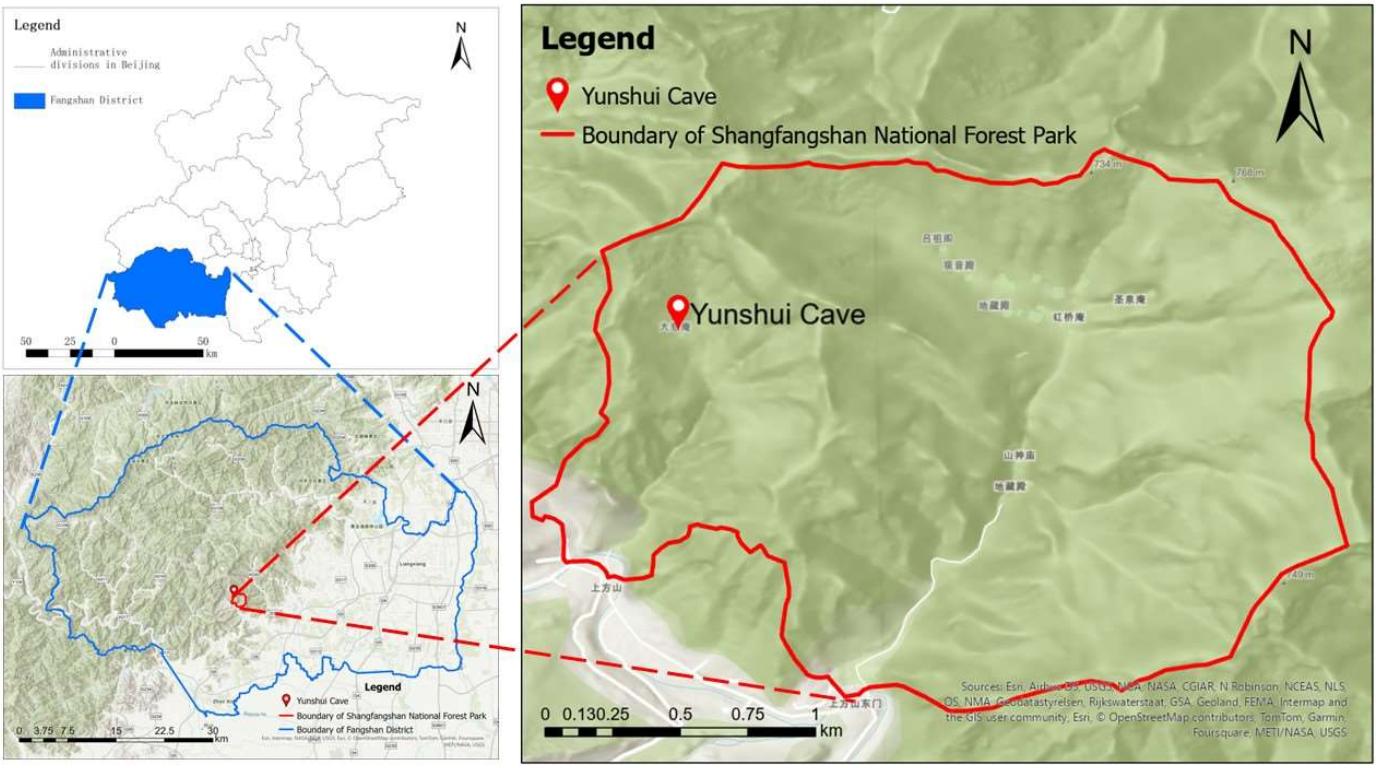

Figure 1. Location map highlighting the precise location of Yunshui Cave in Shangfang Mountain, Beijing, China. The non-English terms in the figure are the Chinese names of the locations.

The structure of Shangfang Mountain is complex. As shown in Figure 2 [8], the northern region of China, to which Shangfang Mountain belongs, has developed three major faults from west to east, which control the overall landform of this region. In the case of the Beijing region, the western part of Beijing belongs to a low mountainous area with developed, folded strata. The tectonic movement of the strata has led to the formation of various canyons, peaks, and karst caves in Shangfang Mountain.

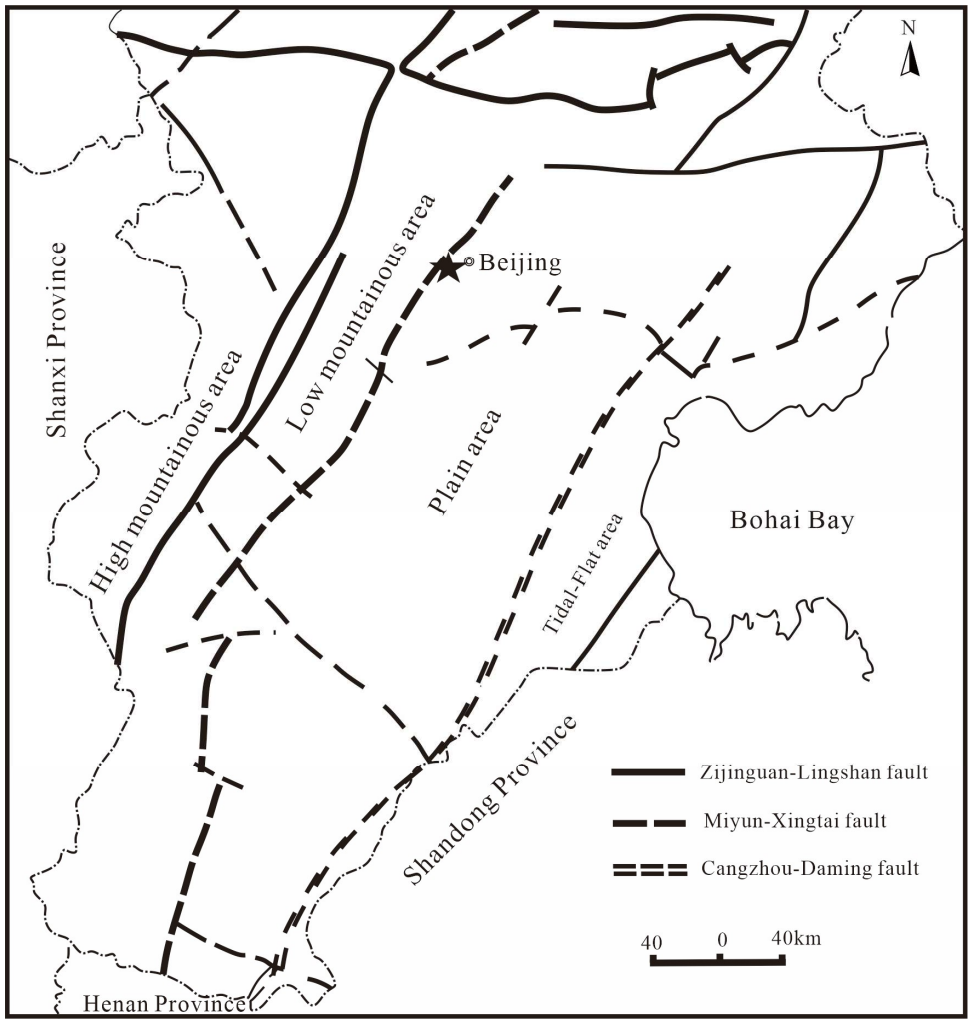

Figure 2. Distribution map of major faults in North China.

The area of Shangfang Mountain is a typical area of karst landform in northern China [9]. In this geological environment, the independent underground space of the underground pipe formed by karst rock (possibly partial erosion) with a certain diameter or a long continuous runoff space is called a karst cave [10], such as Yunshui Cave. The formation of karst landscapes and caves in this area is mainly related to the geological rock combinations, mineral composition, and tectonic processes developed in this area. The formations that form karst caves in this area, exposed in ascending order from older to newer, include the Middle Proterozoic Jixian System Wumishan Formation (Jxw), the Middle Proterozoic Jixian System Hongshuizhuang Formation (Jxh), and the Middle Proterozoic Jixian System Tieling Formation (Jxt) [8]. The geological map of Shangfang Mountain and the location of Yunshui Cave are shown in Figure 3 [11].

The Wushan Formation (Jxw) is mainly composed of grayish white medium-thick limestone, thick dolomite with flint strips, and thick stromatolite dolomite. The Hongshuizhuang Formation (Jxh) is mainly composed of black-green shale and slate, interbedded with thin dolomite, thin sandstone, and elliptical carbonate nodules. The Tieling Formation (Jxt) is mainly composed of thin-layered glauconite-bearing limestone, dolomitic limestone, and manganese-bearing dolomite. Both dolomite and limestone are carbonate rocks. Dolomite belongs to the magnesium-rich carbonate with a chemical composition of $CaMg[CO_3]_2$, while limestone belongs to the calcium-rich carbonate with a chemical composition of $CaCO_3$. They are all soluble rocks, which chemically react with water to form bicarbonate, blend into the water, and gradually form karst caves along the joints where they are dissolved. When the bicarbonate entering the water meets the right conditions, it

will release carbon dioxide, causing the carbonate to re-precipitate. This process can form stalactites of various shapes, such as stalagmites.

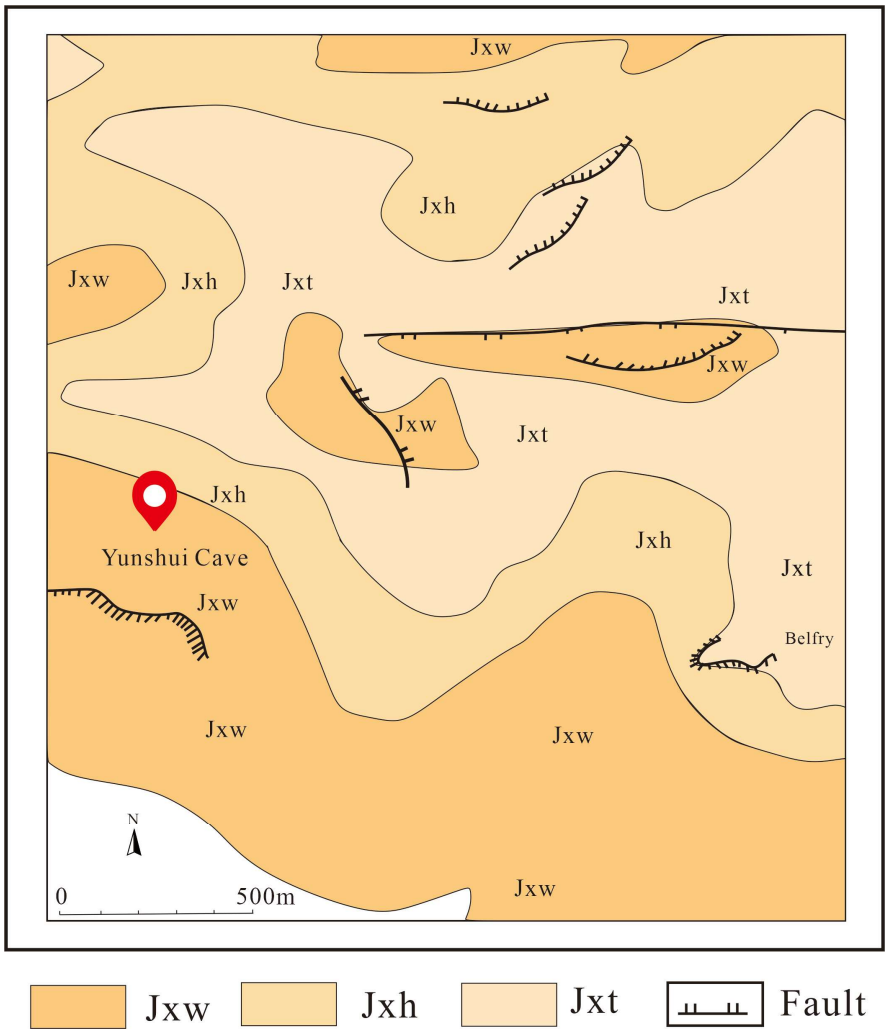

Figure 3. The geological map of Shangfang Mountain and the location of Yunshui Cave. The geological strata include the Middle Proterozoic Jixian System Wumishan Formation (Jxw), the Middle Proterozoic Jixian System Hongshuizhuang Formation (Jxh), and the Middle Proterozoic Jixian System Tieling Formation (Jxt).

The outspout strata of Yunshui Cave are dolomitic limestone and dolomite of the Wumishan Formation. The thin slate and dolomite of the Hongshuizhuang Formation appear on the tunnel wall of the entrance corridor of Yunshui Cave. The tops of the first four karst caves are made of thin limestone from the Tieling Formation. The rock formation of Yunshui Cave is gentle, and the main body of the cave is developed in the Wumishan Formation and the Hongshuizhuang Formation. The cross-sectional view of Yunshui Cave is shown in Figure 4 [11]. The rock joints in Yunshui Cave are well developed, and the measured joints in the cave are mainly near north–south and near east–west directions, and many cave walls are the rupture surfaces of these joints. In fact, it is the north–south joint that controls the extension direction of the cave, and the east–west joint restricts the lateral development.

Since prehistoric times, karst caves have been an important part of the cultural landscape in many parts of the world, and they are widely used as various cultural environments, including but not limited to residence, religious rituals, and refuge [11]. Similarly, Yunshui Cave is not only a famous high-altitude karst cave in the suburbs of Beijing but also a famous Buddhist tourist destination in North China [12], attracting many scholars who come there to conduct cultural and geological research. Tang Shaoguo [13] and Luo Zhao [14] conducted cultural investigations of Yunshui Cave in the 1990s, and geological research on Yunshui Cave began as early as the beginning of the 20th century. At the beginning of the last century, G. Bouillard made many investigations of the Yunshui Cave. In the early 1980s, Ye Junlin et al. revisited the cave and compared the new measurement data with the old data. Huang Wanbo et al. also visited the cave to study the formation of vertebrate fossils [15]. The Yunshui Cave in Shangfang Mountain is a place of high cultural and scientific value.

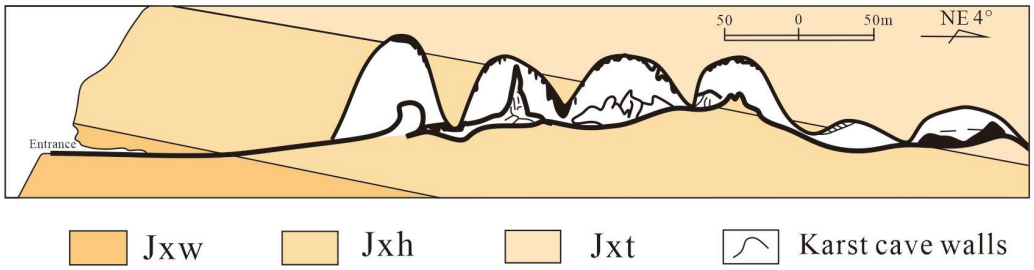

Figure 4. The cross-section map of Yunshui Cave shows the distribution of strata. The strata include the Middle Proterozoic Jixian System Wumishan Formation (Jxw), the Hongshuizhuang Formation (Jxh), and the Tieling Formation (Jxt).

1.2. Selection of the LiDAR Technical Method

Due to the fact that karst caves are mostly distributed in densely forested areas with few human footprints, the transportation of large equipment is inconvenient. At the same time, the roads inside the caves are narrow and rugged, and the lighting is inconvenient. In the past, related measurement work could only be carried out using simple step estimation methods or simple rope measurement methods. Although these methods can also effectively obtain measurement results, the operation is relatively difficult, the accuracy is poor, and the efficiency is also relatively low. It can only roughly measure simple data, such as cave depth, and cannot carry out more precise and detailed data measurements [16].

Nowadays, terrestrial laser scanning (TLS) and 3D photogrammetry techniques are used in caves with archaeological value [17], obtaining data that can be used for 3D modeling [18]. The obtained data can be used for archaeological research and can also help reveal the development process and hydrological evolution of these caves [19]. Ground penetrating radar (GPR) and microgravimetric measurements can be used to map underground karst features [20] or detect buried structures [21]. The passive seismic standing wave method can also be used to study underground caves, which is based on the effect of the generation of standing waves by microtremor in the space between the earth's surface and the cave roof [22]. In addition, underwater caves can be measured using handheld echosounders [23]. However, terrestrial laser scanning operates on the ground, and its range is limited by ground obstacles and occlusions. The accuracy of ground-penetrating radar may diminish under complex geological conditions. The passive seismic standing wave method involves a lengthy data collection cycle, complex signal processing, and low research efficiency. Although handheld echosounders are portable and practical, unskilled operation can result in measurement errors or inaccurate results.

LiDAR measurement, as a new technology, is a convenient handheld scanning device and an active laser measurement method that does not require lighting conditions. It provides a more satisfactory response to the inconvenience caused by traditional methods for investigating and measuring karst caves [24]. It can achieve centimeter-level omnidirectional measurement technology with up to 300,000 points per second and has broad application space in karst cave measurement. Simulating natural phenomena using 3D technology can deepen our understanding of the environment, and dense 3D point clouds can be used as high-precision input datasets [25].

LiDAR technology, combined with GIS, can quickly provide more accurate and comprehensive geological and topographic data [26].

In the field of remote sensing and photogrammetry in the 21st century, LiDAR technology is one of the most innovative technologies [27]. The laser scanner loaded with LiDAR emits fast pulse signals with high measurement efficiency. It can obtain hundreds of thousands of precise measurement points per second, and the signal penetration ability is also very strong. It can penetrate vegetation cover and has rich echoes, which can transmit vegetation information and ground information back. It can be widely used in mountainous and hilly areas [28,29]. In recent years, scholars around the world have utilized LiDAR measurement technology to conduct applied research in multiple fields, including in the drawing of cave maps [30,31], which has both guiding significance and reference value for our research. In addition to these applications of the technology, some scholars have used the high-resolution digital elevation model obtained by LiDAR to describe and study the karst landform [32–34], which has also inspired us in our survey. In China, it is used with good results in geological mappings and engineering surveys [28], as well as for geological disaster identifications [35], geological modeling [36], and other aspects.

1.3. The Significance of the Yunshui Cave Investigation

The Shangfang Mountain Yunshui Cave has long been famous. It is one of the earliest locations in China where modern geological surveying and mapping were carried out [12]. However, the last scientific research conducted in Yunshui Cave was in the 1980s, and there has been no further scientific investigation related to its surveying and mapping for over 40 years. Due to the limitations of traditional geological investigation and field measurement tools, there has been no precise data that can be specifically explored and analyzed for the specific depth, width, and development characteristics of the Yunshui Cave. Therefore, the new mode of Shangfang Mountain Yunshui Cave scientific research conducted using the new LiDAR scanning technology is an example of groundbreaking cave research work that has significant research significance in the scientific investigation history and geological research methodology of Shangfang Mountain Yunshui Cave.

This time, the use of LiDAR technology as a new mode of scientific research has greatly improved our understanding of the Yunshui Cave in Shangfang Mountain. In an environment with insufficient light and poor visibility inside the cave, we obtained comprehensive internal data and established a fully digital three-dimensional model of the Yunshui Cave, revealing its rich geological features and providing important data support for subsequent protection of the cave as well as for its development and utilization. This study provides a foundation for future explorations of the Yunshui cave and highlights the potential for LiDAR techniques to enhance our understanding of complex geological structures such as caves. At the same time, it has also opened up new research methods and technical means for the field of geological survey in China.

2. Materials and Methods

This study uses LiDAR technology, and the research process is shown in Figure 5.

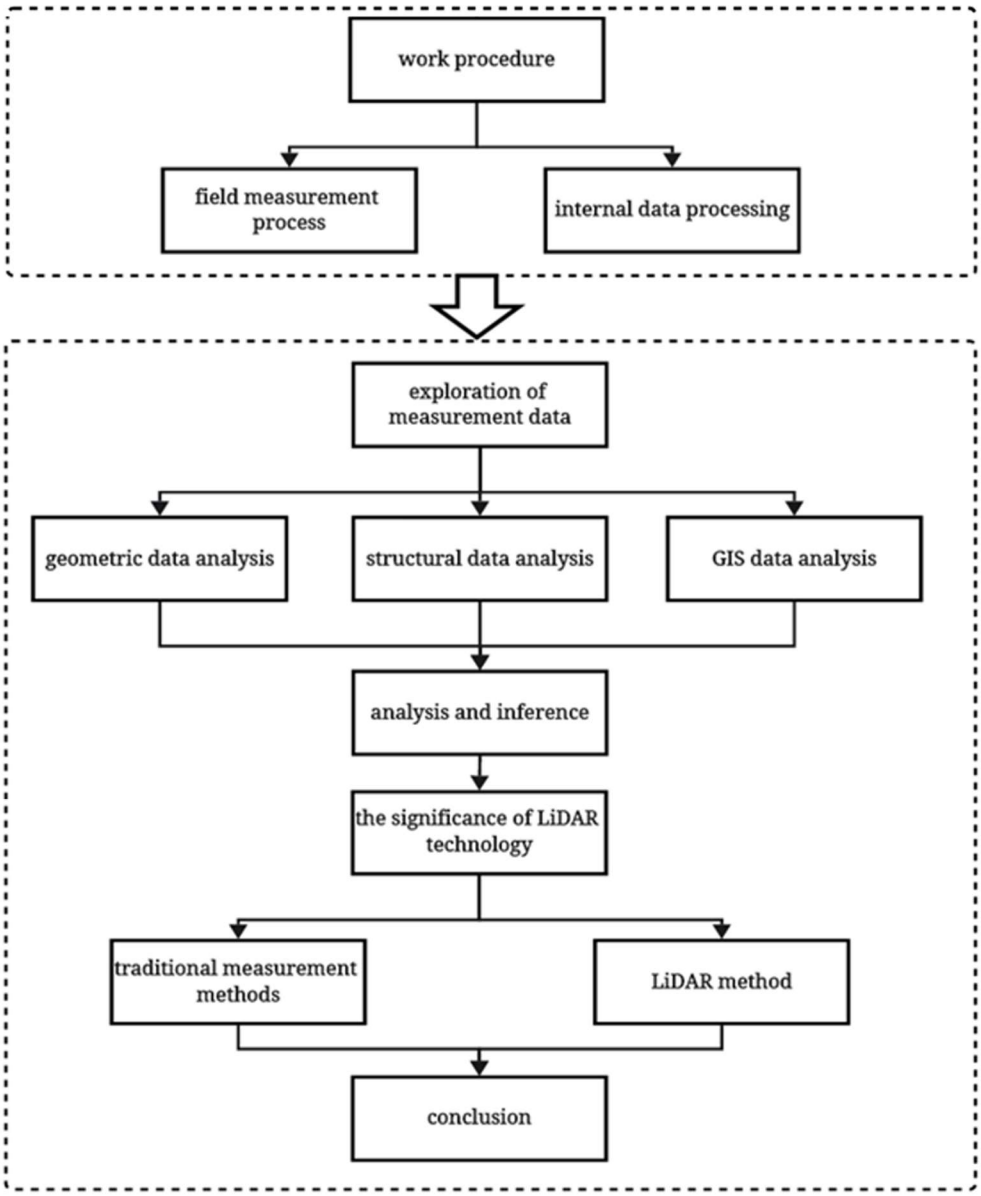

Figure 5. Study process of this article.

2.1. Measuring Method

LiDAR is a radar system that has been constructed to detect the position and speed of the target [37]. Three-dimensional laser scanning technology, as a kind of high-efficiency, high-precision surveying and mapping technology, can scan the underground mine or cave and obtain the corresponding 3D space data, thereby improving the efficiency of its development and application of the results it provides. For example, by using 3D scanning data to construct 3D models of mineral caves and karst caves, their volumes and profile lines can be calculated, which can lead to an accurate measurement of cave volume and other applications [38].

A ZEB-HORIZON handheld 3D scanner (Figure 6) was used for this measurement. ZEB-HORIZON handheld 3D scanner is a product of FARO SINGAPORE PTE. LTD., located in Singapore City, Singapore. ZEB-HORIZON was measured at 100 m at 300,000 points per second with an accuracy of 1–3 cm. At the same time, with the use of powerful SLAM technology, highly accurate models can be built up in remote areas with poor GPS, such as underground goaf, tunnels, karst caves, indoor buildings, and forest environments [39].

The technical parameters related to ZEB-HORIZON and this experiment are shown in Table 1.

Figure 6. A ZEB-HORIZON handheld 3D scanner for LiDAR measurement.

Table 1. Technical parameters of ZEB-HORIZON.

Parameter	Value
Scope	100 m (feature < 40 m)
Protection level	IP54
Process mode	Reprocessing
Point cloud color	Yes
Refer to images	Yes
Number of points scanned per second	300,000
Number of sensors	16
Relative accuracy	1–3 cm

ZEB-HORIZON is small, lightweight, and can measure with high efficiency while being held by a person who is walking. It can quickly and comprehensively obtain data in a short period of time. Meanwhile, ZEB-HORIZON can flexibly adjust the angle and height to expand the scanning range or to enter difficult-to-reach spaces (such as ceiling gaps). By connecting ZEB-HORIZON to GeoSLAM, it can be lifted to drop down to hard-to-access areas (e.g., manholes). ZEB-HORIZON can also be mounted on drones and taken to the sky to fully cover all areas.

2.2. Working Procedures

The main contents of this survey work are as follows:

1. Getting data. A ZEB-HORIZON handheld 3D scanner was used to obtain the high-precision three-dimensional point cloud model data of the Yunshui Cave in Beijing, including its shape, size, surface characteristics, and other information, all of which provided a basis for subsequent modeling.
2. Point cloud streamline. Due to the large amount of original point cloud data, resulting in slow processing speed and low operation efficiency, the octree method is used for point cloud resampling to reduce the amount of data. Octree is a spatial segmentation data structure used for the efficient storage and querying of objects in three-dimensional space.
3. Point cloud registration. Select and pick up some points from the original point cloud data and convert the coordinates of the point cloud data from the relative coordinate system of the scanner itself to the absolute geodetic coordinate system required by the project. By doing so, we are ensuring that they are fully presented in a unified coordinate system.
4. Point cloud denoising. First, the software is used for semi-automatic denoising, and then the key parts are manually denoised to improve the data accuracy.

5. Point cloud modeling. Based on the obtained three-dimensional point cloud model data, the three-dimensional effect model of the karst cave is established, and a series of analyses of the model cutting section and volume calculation are conducted.
6. Planar analysis. Through the vector editing and labeling of entity elements, the vectoring of major key features is completed.
7. By constantly scanning the surface of an object, LiDAR can obtain large areas of high-resolution three-dimensional point cloud data on the surface of the subject object [40]. These data can not only describe the overall structure of the tested entity but also show the local morphological characteristics. Through point cloud collection, it can also reconstruct a 3D model and restore the original shape of the object. Therefore, through the processing and analysis of the point cloud data, we can obtain a lot of information, such as the contour shape of the tested entity, the surface texture, the relative positional relationship between objects in the point cloud data, etc. The specific operation procedure is shown in Figure 7.

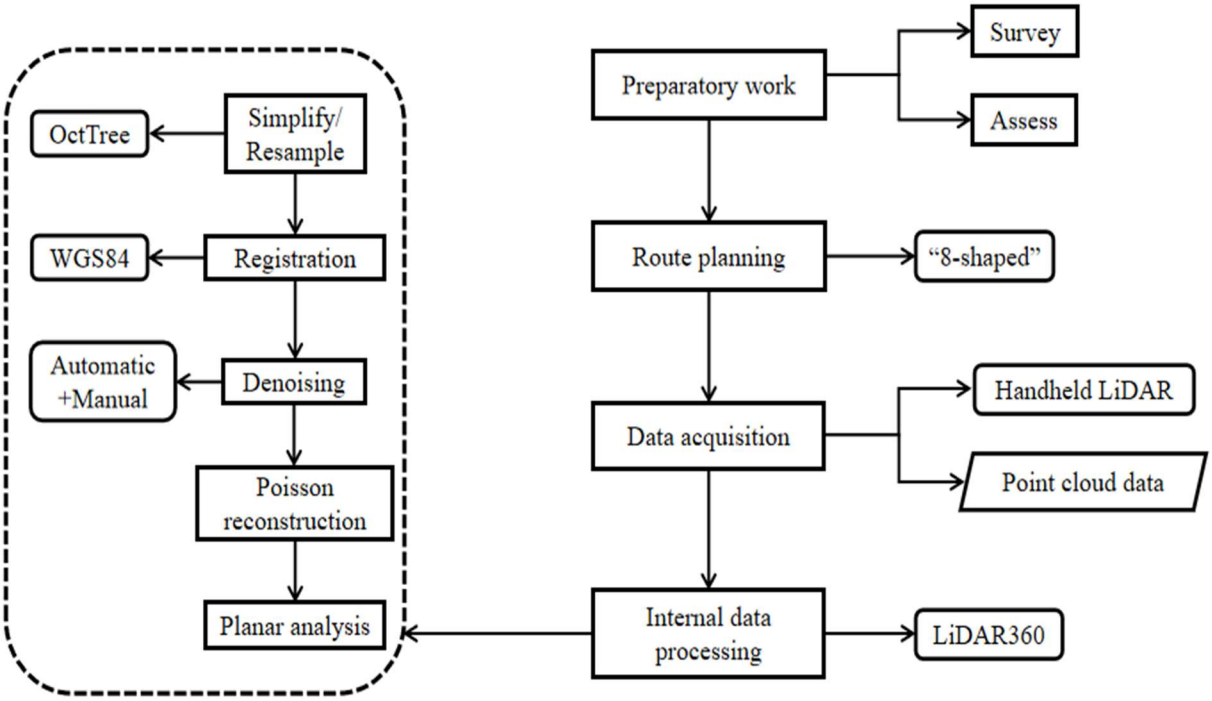

Figure 7. Workflow.

2.2.1. Preparatory Work

First of all, an internal investigation and evaluation of the karst cave should be carried out. The main characteristics, channel width, and height of the karst cave are determined in order to guide the rational layout and route planning of the scanner. Then, according to the survey results, the karst cave is divided into different scanning areas. Considering the field of view and the extent of the laser scanner, ensure that each area can be adequately covered by the scan. If there is an area with a large elevation difference in the cave, consider using elevation measurement tools, such as level meters or laser rangefinders, to record the elevation changes within the cave to better capture the topographic features.

2.2.2. Route Planning

Based on the survey results, develop a scanning path to ensure the uniform distribution of point cloud data, avoid path intersections or paths that are missing, and ensure that the entire karst cave can be scanned. For the scene of entering the cave from outdoors, after initiating the cave, directly enter the cave along the side of the cave for measurement. In the field operation, the operation speed of the hand-held scanner should be slowed down

to ensure that all parts of the cave can be scanned. At the same time, the "8-shape" route (Figure 8) can be used when scanning, and instead of repeating any part of the scanning, try to follow a closed-loop route. When encountering large measurement areas or obstacles, measurements can be carried out in zones and stages.

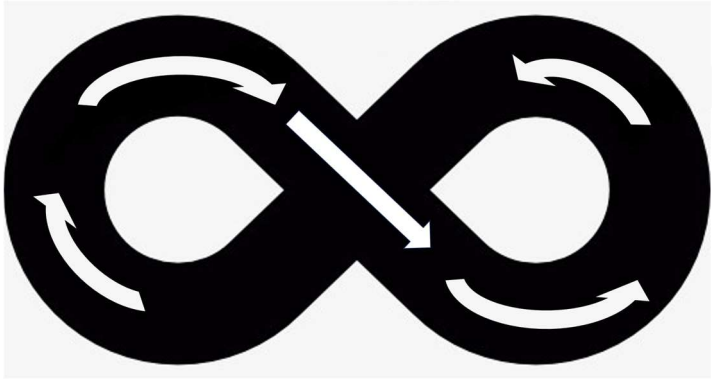

Figure 8. The "8-shaped" route used in LiDAR scanning.

2.2.3. Data Acquisition

1. Install the equipment, boot the camera, power the devices, and select an open position to initialize the equipment. During the initial phase, the laser faces the opening.
2. After the initialization, slowly pick up the equipment, collect the data according to the planned route, and keep the equipment as stable as possible during the collection process.
3. After the data collection, hold the equipment in place, wait for the laser to stop turning, finish the laser data collection, and manually press the camera button to stop recording.
4. Use the data transmission line to connect the battery box and the computer terminal, set up the computer IP, and export the collected data results.

2.2.4. Internal Data Processing

Based on the initial underground roadway point cloud data acquired by the 3D laser scanner, point cloud processing software is needed to carry out the identification and analysis of the structural surface. This study chose LiDAR360 V7.2 for point cloud processing. Other software for processing point cloud data includes CloudCompare, Globalmapper, etc. The reason for choosing LiDAR360 V7.2 over other software is that it has high work efficiency in situations with large amounts of data, with over 10 point cloud processing and AI algorithms, as well as over 700 powerful and flexible functions. It achieves multi-source massive data visualization, 2D and 3D integrated display, profile analysis, measurement selection, point cloud data quality inspection, multi-point cloud classification, data stitching, and other functions.

(1) Point cloud streamline

A 3D laser scanner can obtain a large amount of point cloud data in a short period of time. The higher the scanning resolution and volume required for the target object, the larger the amount of point cloud data obtained. A large amount of point cloud data will occupy a large amount of system memory in storage, operation, display, output, etc., resulting in slow processing speed and low operating efficiency [41]. Therefore, the point cloud data should be reduced according to the entity structure; otherwise, useful information will be lost. The core idea is to maximize the geometric structure features of the research target through the fewest points [42].

The streamlined approach to point cloud data can be roughly divided into two categories [43]. The first is based on spatial division, and the second is based on a point-based reduction algorithm. The octree structure used in this study to partition the topological

structure of point cloud data is a common method of point cloud simplification based on spatial partitioning. The core idea is to divide the point cloud data into an octree structure, treating each node as a small spatial unit and using the difference between the normal vector angle and the average normal vector of the point cloud within each spatial unit as a judgment basis, deleting point clouds with significant differences in normal vectors, thereby achieving simplification of the point cloud data. The octree structure is sufficiently flexible and efficient to effectively process large amounts of data in point clouds and can retain important features of point clouds. In LiDAR360 V7.2, select resampling, where the sampling type is octree; this method is uniform sampling, with a sampling rate of 30%, which results in Figure 9.

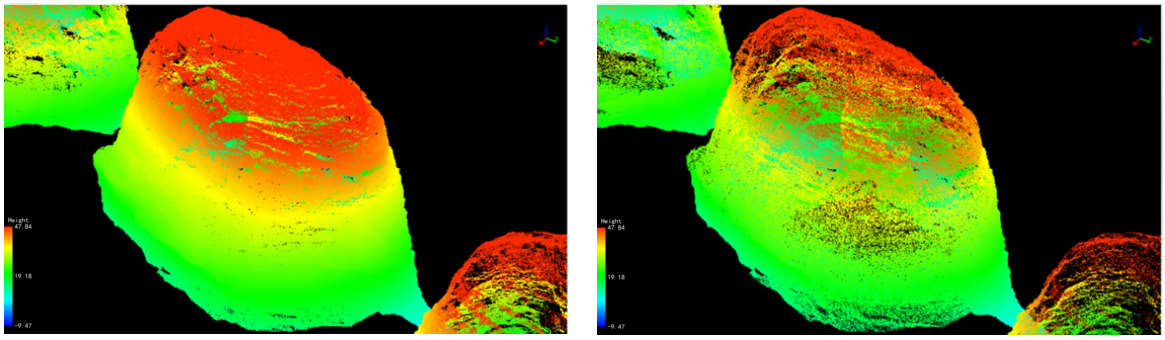

(**a**) (**b**)

Figure 9. (**a**) The point cloud data before streamlining in LiDAR360 V7.2, with a large amount of data; (**b**) The point cloud data after streamlining in LiDAR360 V7.2, using the octree method to reduce data volume.

(2) Point cloud registration

The point cloud data obtained from 3D laser scanning measurements is based on the coordinate system of the instrument itself. When using a 3D laser scanning measurement system to scan the three-dimensional morphology of underground karst caves, it is necessary to convert the obtained laser point cloud data to the geodetic coordinate system. Point cloud registration is the process of collecting three-dimensional point cloud datasets from different coordinate systems. This is achieved through spatial geometric transformations (rotation and translation) into a unified coordinate system, forming complete point cloud data. Essentially, it is the process of transforming point cloud data into spatial coordinates [43].

In this study, we used LiDAR360 V7.2 for geographic registration, importing the unprocessed point cloud data through the data registration function, and selecting some points as the reference for registration. Having done this, we pick up their geographic coordinates and accurately define their position in the WGS84 coordinate system for registration. We have selected four points for geographic registration. The actual location of the registration points corresponds to their location in LiDAR360 V7.2, as shown in Figure 10. Point 1 and Point 2 are located on both sides of Yunshui Cave's entrance. Due to the lack of openness in front of Yunshui Cave, we have set up Point 3 and Point 4 on both sides of the temple outside the entrance of Yunshui Cave. The geographical coordinates of the registration points are shown in Table 2. The RTK (real-time kinematic) plane accuracy of the equipment used for measuring registration points is ± (8 mm + 1 ppm). Figure 11 is a photo of our work at Point 4.

Table 2. Reference point coordinates.

PointID	Name	WGS84 X	WGS84 Y	WGS84 Z
1	zd1	−2,140,448	4,425,819	4,050,597
2	zd2	−2,140,447	4,425,822	4,050,598
3	zd3	−2,140,442	4,425,832	4,050,582
4	zd4	−2,140,455	4,425,827	4,050,583

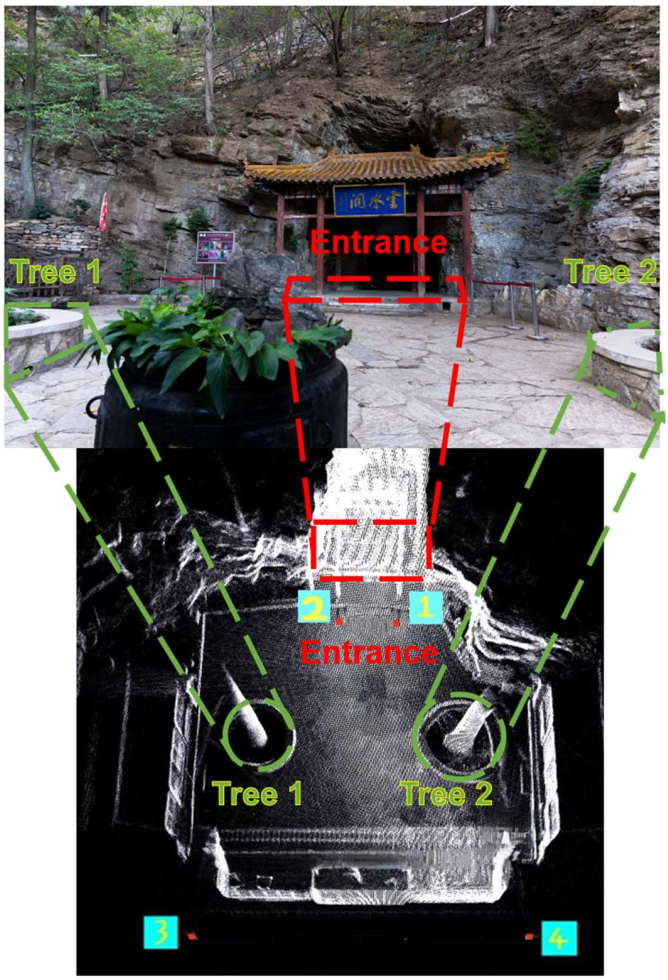

Figure 10. The actual location of the registration points corresponds to their location in LiDAR360 V7.2.

Figure 11. Measuring Point 4 for geographic registration.

(3) Point cloud denoising

When obtaining the original point cloud data of the three-dimensional laser scanner, the noise in the data cannot be avoided due to the influence of equipment, environment, and other factors. Noise will affect the accuracy of the point cloud data and the efficiency of the subsequent feature extraction, surface reconstruction, and other application processing, so it is necessary to filter and denoise the point cloud before the application processing [42].

Method 1: Automatic software elimination

With the increase in point cloud processing software, more and more commercial software provides the denoising function of point cloud. In LiDAR360 V7.2, import the calculated karst cave point cloud data into LiDAR360 V7.2for semi-automatic denoising, and set the parameters in the software mine module denoising option. Figure 12 shows the comparison before and after point cloud denoising.

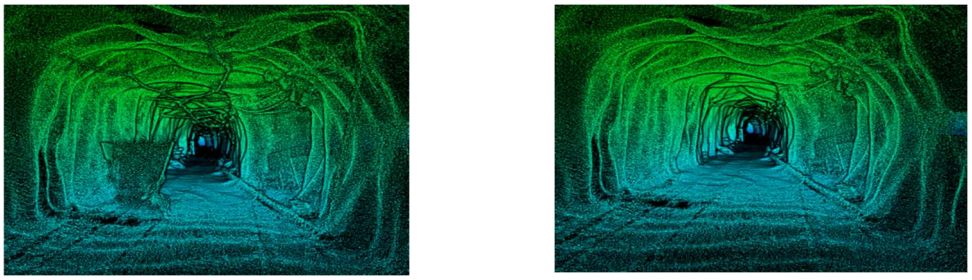

(**a**) (**b**)

Figure 12. (**a**) The point cloud data before denoising in LiDAR360 V7.2 contains noise that affects measurement accuracy; (**b**) The point cloud data after denoising in LiDAR360 V7.2.

Method 2: Manual elimination

For obvious and relatively isolated noise points, such as trees and buildings, they can be manually selected and eliminated [44]. In LiDAR360 V7.2, profile editing can be opened and noise can be manually removed, as shown in Figure 13. The process of this elimination method is relatively simple, and the accuracy is also relatively high. The disadvantage is that only a small amount of data can be processed, and the efficiency is relatively low.

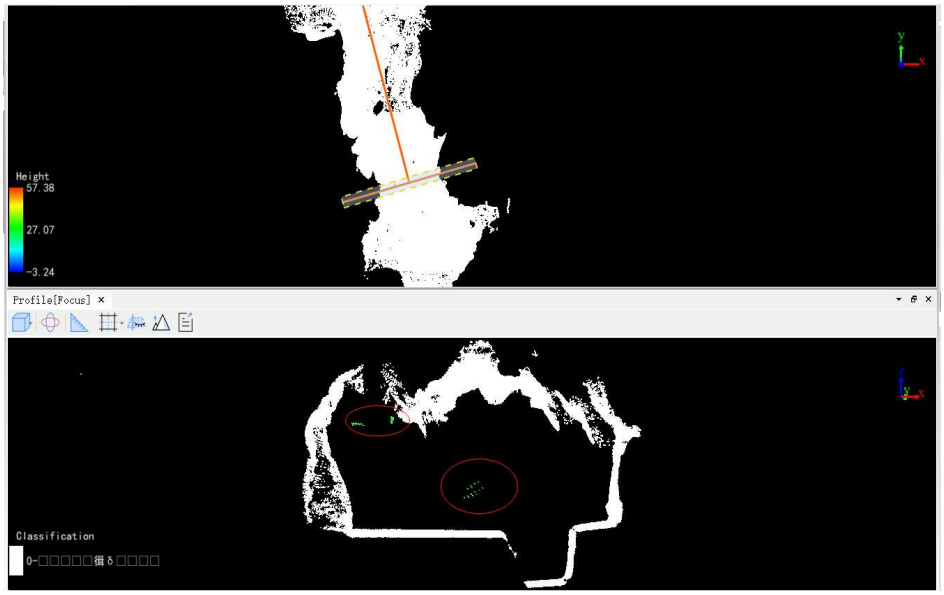

Figure 13. Manually remove obvious and relatively isolated noise points in LiDAR360 V7.2. The thick orange line in the figure indicates that manual elimination is being carried out. The interior of the red circle is the noise points to be manually removed.

(4) Poisson reconstruction

The Poisson reconstruction is a 3D surface reconstruction method based on the Poisson equation [45]. The basic idea of Poisson surface reconstruction is as follows: input the point cloud data containing the normal line, the normal line representing the direction pointing inside and outside the object, to obtain the vector field $\vec{V}$ of the unknown object M. Assuming that all points are located on or adjacent to the surface of the unknown object M, there is an indicator function $X_M : R^3 \rightarrow R$:

$$X_M(p) = \begin{cases} 1, p \in M \\ 0, p \notin M \end{cases} \quad (1)$$

Wherein $p = p(x, y, z)$ is a point in space. Meet: The gradient of this indicator function ∇X_M is approximated by the vector field $\vec{V}$, namely $\min_X \left\| \nabla X - \vec{V} \right\| \Rightarrow \nabla X \approx \vec{V}$. That is to say that the indicator function X is an implicit function related to an object, 1 a scalar field in space, and the gradient of the sampling point is the normal vector of the isosurface of the point.

The bilateral action divergence operator ∇ is transformed into a Poisson equation:

$$\Delta X = \nabla \cdot (\nabla X) = \nabla \cdot \vec{V} \quad (2)$$

Using the finite element method, we may obtain the expression X of the implicit function. Based on the angular values of the voxels $X(p)$ and the equivalence γ of the unknown object M, the isosurface was extracted from the voxels using the MC algorithm to output the triangular mesh, where p represents the coordinate position of the corner point. The process diagram of a Poisson reconstruction is shown in Figure 14. The far left side of the graph is the point cloud data with direction, which is called the oriented point. The second from the left of the graph indicates the gradient of the function, and the third from the left is the indicator function. The far right side of the image is the surface obtained through Poisson reconstruction.

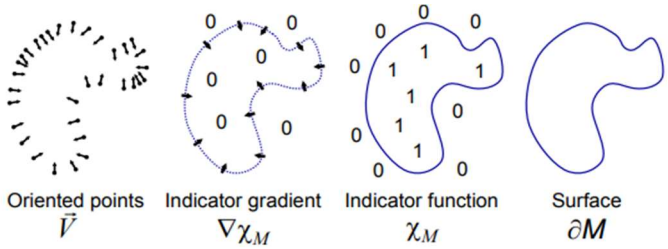

Figure 14. A process diagram of the Poisson reconstruction. From left to right are the orientation points, the gradient of the function, the indicator function, and the surface obtained through Poisson reconstruction.

A poisson reconstruction was performed in LiDAR360 V7.2 using the processed point cloud data. The normal calculation was first performed to measure the average point spacing of 0.05 m, so that the optimal search radius of 0.25 m was chosen. By performing a neighborhood search on each point to obtain adjacent points, the normal direction is calculated based on these points, and the minimum spanning tree is used to optimize the consistency of the normal direction. The minimum spanning tree algorithm divides the point cloud into an adjusted normal vector point set U and an unadjusted normal vector point set W, and then selects the point u with the lowest weight in the point set U and the point w with the lowest weight in the point set W. On the premise of ensuring that the normal vector direction between the two does not change abruptly, the normal vector direction of point w is determined by the normal vector direction of u. The direction of normal vector propagation is determined by the method of selecting weights. First, a seed point is extracted to ensure that the normal vector direction of that point is correct. Then, propagation is carried out in the direction with the minimum weight.

For each new point propagated, the normal vector of the new point is modified, and the point sets U and W are updated according to the principle of no sudden changes in the normal vector direction until all points are traversed. Ultimately, a tree will be formed that includes all points and minimizes the sum of edge weights, completing the consistency optimization of the normal direction [46]. Then, the Poisson modeling of the calculated point cloud is performed, setting the minimum number of points in each node as 1.5, the point weight as 2.0, the resolution as 0.4, and generating a 3D model file in obj format (Figure 15). The height values on the left side of Figure 15 represent the elevation measurement results based on the entrance of the Yunshui Cave in meters. Positive values indicate being higher than the entrance, while negative values indicate being lower than the entrance.

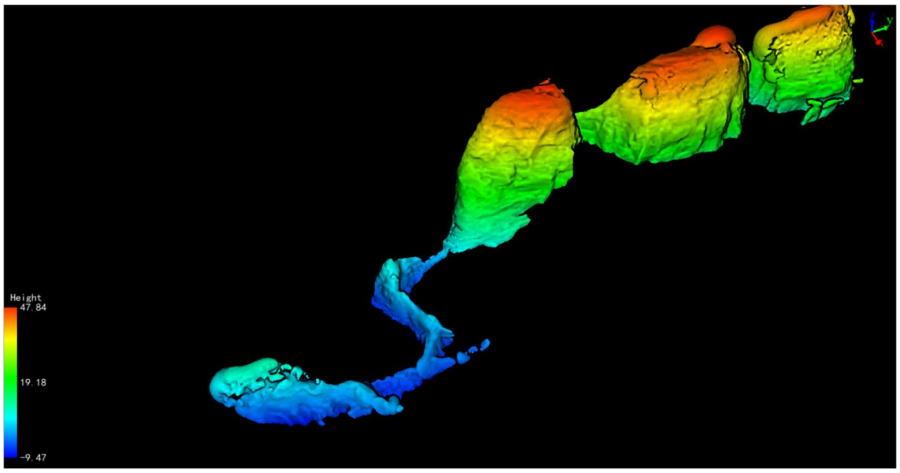

Figure 15. The point cloud data after Poisson reconstruction in LiDAR360 V7.2.

(5) Plane analysis

In Figure 16, use LiDAR360 V7.2's vector editing tool to provide basic entity elements such as points, lines, polylines, rectangles, and polygons to manually edit and annotate key objects. These edits can be managed in a layer-wise manner, facilitating users to organize and analyze vector data. Ultimately, the results of the analysis and editing are presented in a visual way, enabling users to intuitively understand the internal structure and topographic features of the cave.

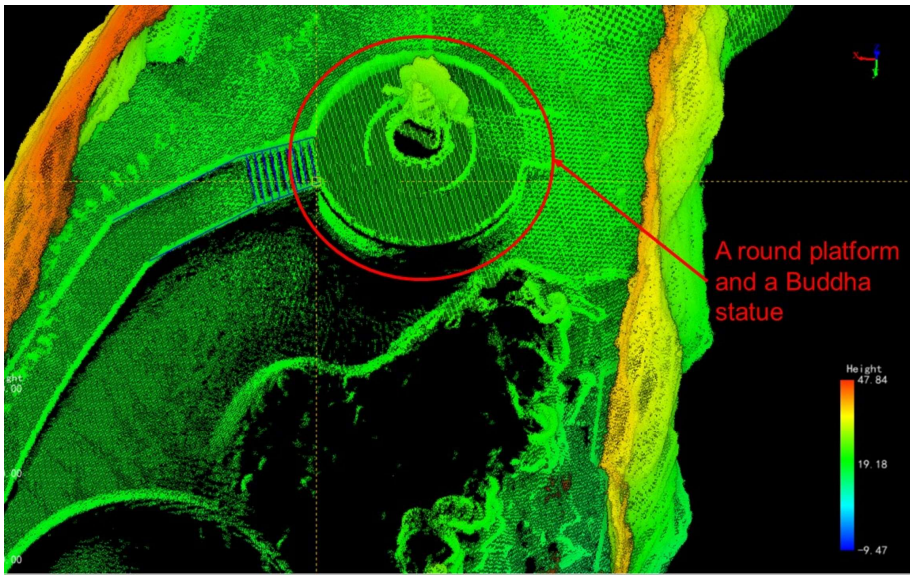

Figure 16. View the internal structure of the cave in LiDAR360 V7.2. There is a round platform and a Buddha statue.

3. Data Exploration Results

3.1. Geometry Analysis of Yunshui Cave Measurement Data

View the point cloud data of the Yunshui Cave in the LiDAR360 V7.2 software. Due to the extension of the entire Yunshui Cave towards the northeast direction, we measure the length and width of each cave not along the north–south or east–west direction but along the main extension direction of each cave. We take the distance between the two farthest points in the main extension direction of each cave as its length. After determining the main extension direction of the cave, we take the distance between the farthest two points perpendicular to the cave in that direction as its width. Finally, we measured the vertical distance from the bottom to the top of each cave to determine its height. In addition, we used the volume measurement tool in LiDAR360 V7.2 to measure the volume of each cave. The volume measurement tool interactively selects the measurement reference plane by selecting data from a file or manually clicking the mouse to calculate the volume of the karst cave. If the volume measurement range is manually selected, the error may be significant. To reduce errors, we measured the volume of the cave multiple times and then calculated the average value.

Six caves have been discovered and opened to the public in Yunshui Cave, and the corridor between the entrance and Cave 1 is 147.13 m long, with an average width of 3.6 m and an average height of 2.8 m. Cave 1 is 66.58 m long, 41.61 m wide, and 46.54 m high, with a volume of 25,870.54 cubic meters, which is the widest and highest cave of the Yunshui Cave. Cave 2 is 52.06 m long, 40.17 m wide, and 35.82 m high, and has a volume of 27,798.43 cubic meters. Cave 3 is 72.15 m long, 34.10 m wide, and 40.13 m high, and the volume is 39,093.09 cubic meters, which is the longest and largest cave of the Yunshui Cave. Cave 4 is 62.33 m long, 30.49 m wide, 40.34 m high, and has a volume of 32,857.45 cubic meters. Cave 5 is 52.51 m long, 12.42 m wide, and 16.11 m high, with a volume of 1300.46 cubic meters, which is the smallest cave in the Yunshui Cave. Cave 6 is 59.35 m long, 15.17 m wide, and 20.92 m high, and has a volume of 4321.65 cubic meters.

The length, width, and height of each cave are shown in Figures 17–19 and Table 3. Figure 17 shows the top view of Yunshui Cave, marking the length of each cave. Figure 18 is also the top view of Yunshui Cave, marking the length of each cave. Figure 19 represents the projection of Yunshui Cave in a north–south direction, marking the height of each cave. The LiDAR image of Yunshui Cave adopts a WGS84 coordinate system, and the outermost periphery of the image represents the horizontal and vertical directions. The north needle and scale bar are marked in the figure. The height values on the left side of the figure represent the elevation measurement results based on the entrance of the Yunshui Cave in meters. Positive values indicate being higher than the entrance, while negative values indicate being lower than the entrance.

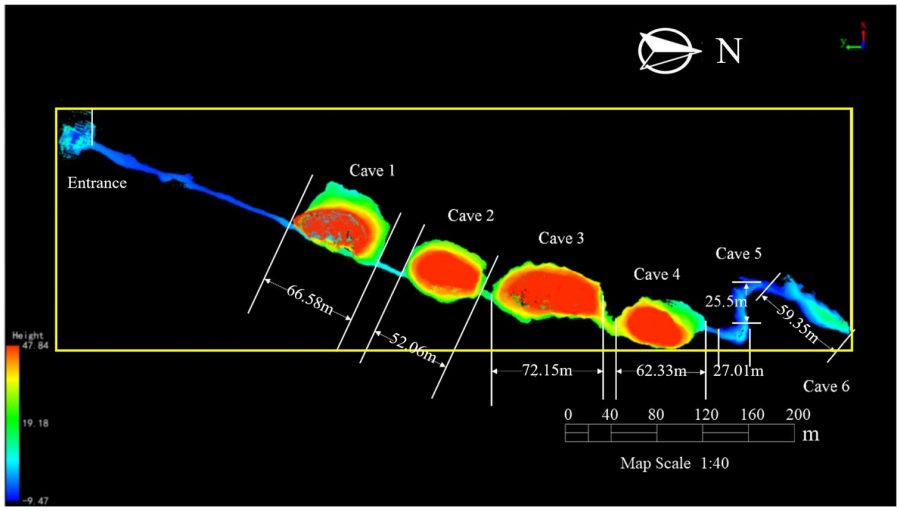

Figure 17. Length of each cave in Yunshui Cave.

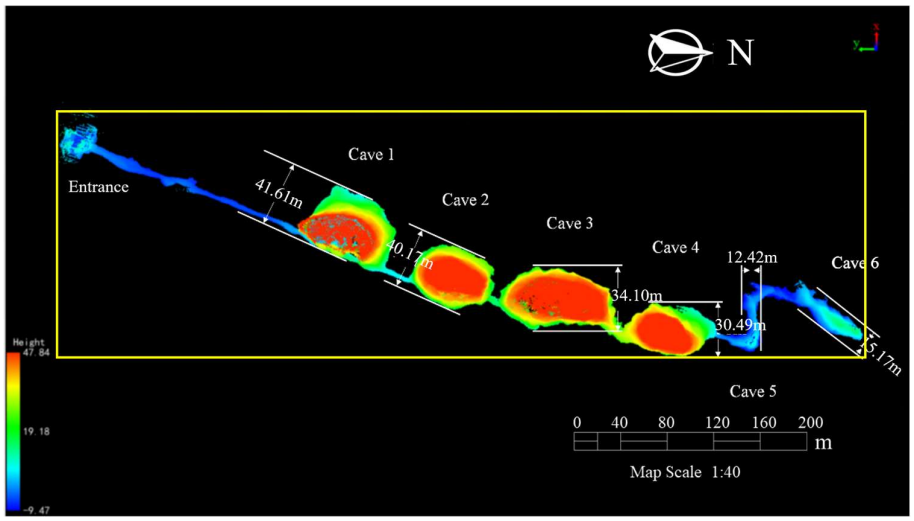

Figure 18. Width of each cave in Yunshui Cave.

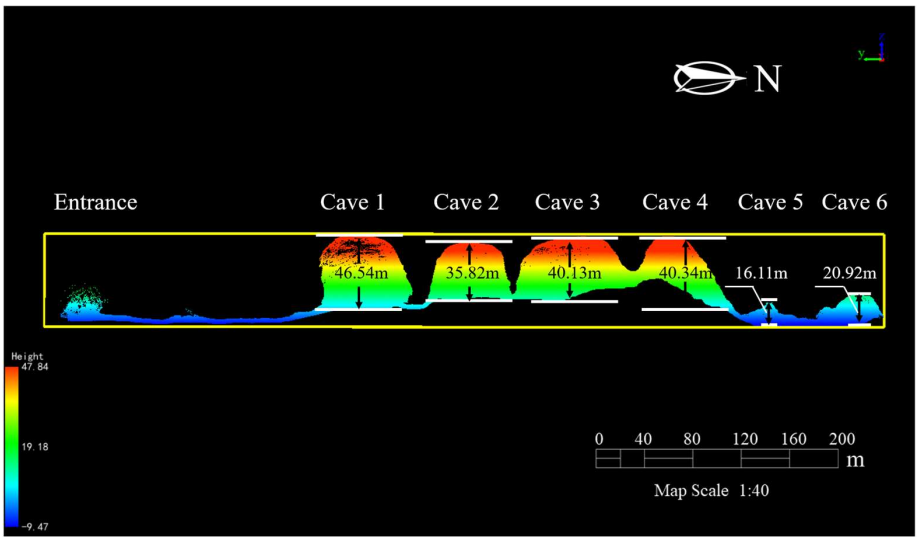

Figure 19. Height of each cave in Yunshui Cave.

Table 3. Geometry data of each cave.

	Cave 1	Cave 2	Cave 3	Cave 4	Cave 5	Cave 6
Length/m	66.58	52.06	72.15	62.33	52.51	59.35
Width/m	41.61	40.17	34.10	30.49	12.42	15.17
Height/m	46.54	35.82	40.13	40.34	16.11	20.92
Volume/m^3	25,870.54	27,798.43	39,093.09	32,857.45	1300.46	4321.65

Yunshui Cave is a tourist attraction, so when conducting scientific measurements, we also hope to determine the shortest path for tourists to visit Yunshui Cave. To achieve this goal, we have established the shortest path for a single cave as the straight-line distance from the entrance to the exit of the cave. Next, we accumulate the shortest path of each cave to calculate the shortest path for tourists to travel throughout the entire cave scenic area. If there is a turn inside the cave, we will measure it in sections. The key to this method is that we recognize that the entrance and exit of a cave may not necessarily be the two farthest points inside the cave, and the shortest path may not necessarily be equal to the length of the cave. Therefore, the length of each cave cannot be simply added up but needs to be remeasured. After measurement, the shortest travel path length of Yunshui Cave

is 566.78 m, as shown in Figure 20. Based on the measurement results, we estimate that the travel time to Yunshui Cave is about half an hour, which can provide a reference for tourists' travel planning.

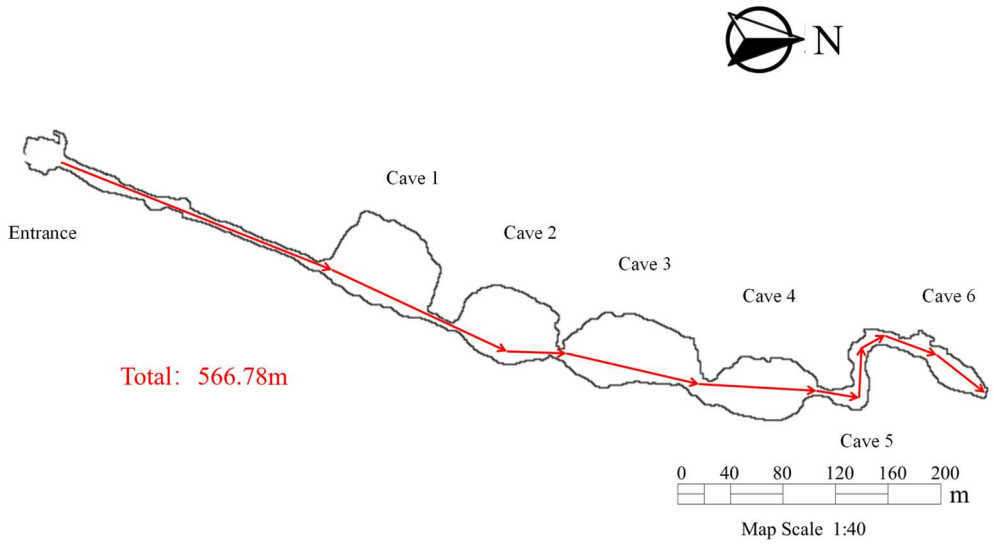

Figure 20. The shortest travel path in Yunshui Cave.

It is worth mentioning that there is a thick and tall upright stalagmite in the center of Cave 2. According to the measurement results of the software, the net height of the stalagmite is 26.9 m, and 31.7 m from the bottom of Cave 2. This tall stalagmite has been metaphorically referred to as the "Sky Pillar" since ancient times, as shown in Figure 21. In the previous scientific investigation of Yunshui Cave, the measured height of this stalagmite was 38 m, which is inconsistent with our measurement results this time. We believe that this is related to the changes in the Yunshui Cave scenic area. The Yunshui Cave underwent scenic area repairs between two scientific examinations. The bottom of Cave 2 was paved with cement, and the height of the observation deck was increased. The lowest point that the measurement personnel can reach now is higher than the lowest point that the previous scientific examination could reach, so the measurement height deviation of the stalagmites is relatively large.

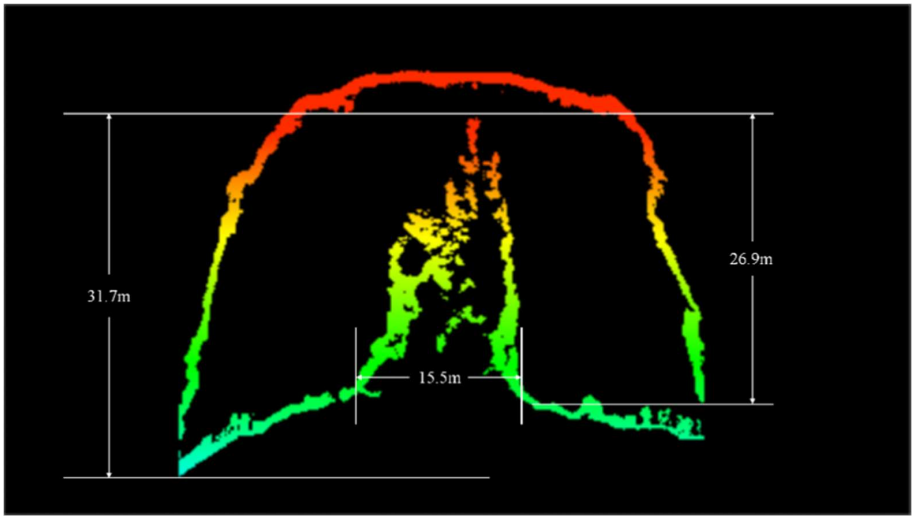

Figure 21. The "Sky Pillar," a famous stalagmite in Yunshui Cave.

Through the LiDAR images, you can also measure the slope of the corridor connecting the various caves in Yunshui Cave. During the development of Yunshui Cave, for the

convenience of visitors, cement or steps were laid on the corridors connecting the caves. The ground of the corridor is basically flat, so we use the corridor ground as a reference surface for slope measurement. As shown in Figure 22, the slope of the corridor from the entrance to Cave 1 is 11°, the slope from Cave 1 to Cave 2 is 30°, the slope from Cave 3 to Cave 4 is 17°, and the slope from Cave 4 to Cave 5 is 26°. The corridors from Cave 2 to Cave 3 and Cave 5 to Cave 6 are relatively flat, with no measured slopes.

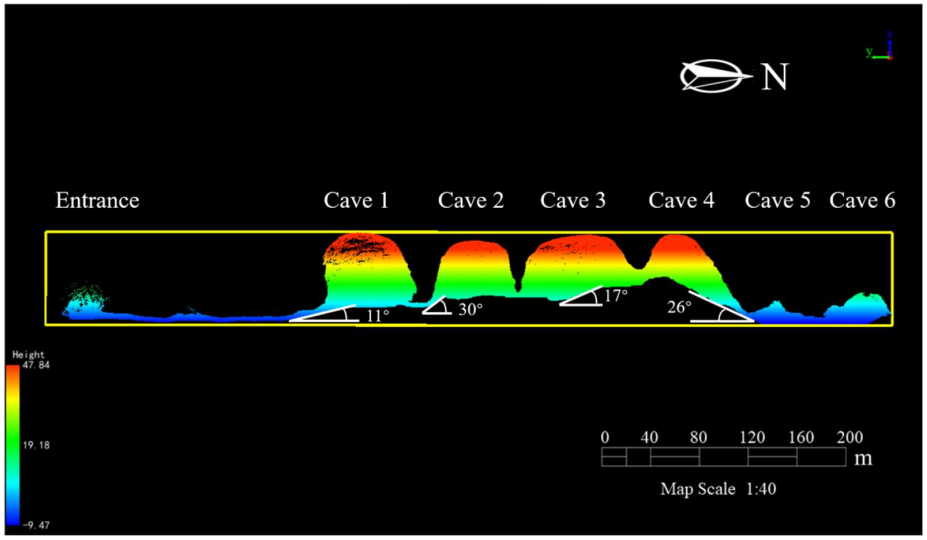

Figure 22. Slope of each corridor in Yunshui Cave.

These data and information are of great significance for the research of Yunshui Cave, and can also provide better support for virtual reconstruction and digital model production. The radar images are further analyzed based on these data.

3.2. Structural Data Analysis of Yunshui Cave

On the basis of the radar image, the plane and cross-section map of Yunshui Cave (Figure 23), the extension section map (Figure 24), and the projection section map in the north–south direction (Figure 25) can be made through ArcGIS 10.8. By adjusting the display mode of point cloud data, the blanking map of each cave can be obtained (Figure 26). In the blank map, we can see the structure and layout of the cave more clearly and observe the cave from various perspectives.

Combined with the radar point cloud image, section maps, and blanking maps, it is found that the six caves in Yunshui Cave are all karst-style caves with uneven walls and relatively flat cave surfaces, making it easy to visit. The first four caves are basically distributed in a straight line, with a bend in Cave 5 and a connection between Cave 5 and Cave 6. Each cave in Yunshui Cave is not distributed on the same level, showing a distribution pattern of "increasing first and then decreasing."

In addition to checking the overall structure of the cave, we can also extract the radar images of each scenic spot to understand the various features and details inside the cave, as shown in Figures 27 and 28. Through further analysis of these radar images, we can also better understand the structure and formation process of the cave. We can explore the formation process of the stalagmites, whether each stalagmite has developed a corresponding stalactite on the cave wall, and even speculate whether the "Sky Pillar" will come into contact with the top of the cave and so on.

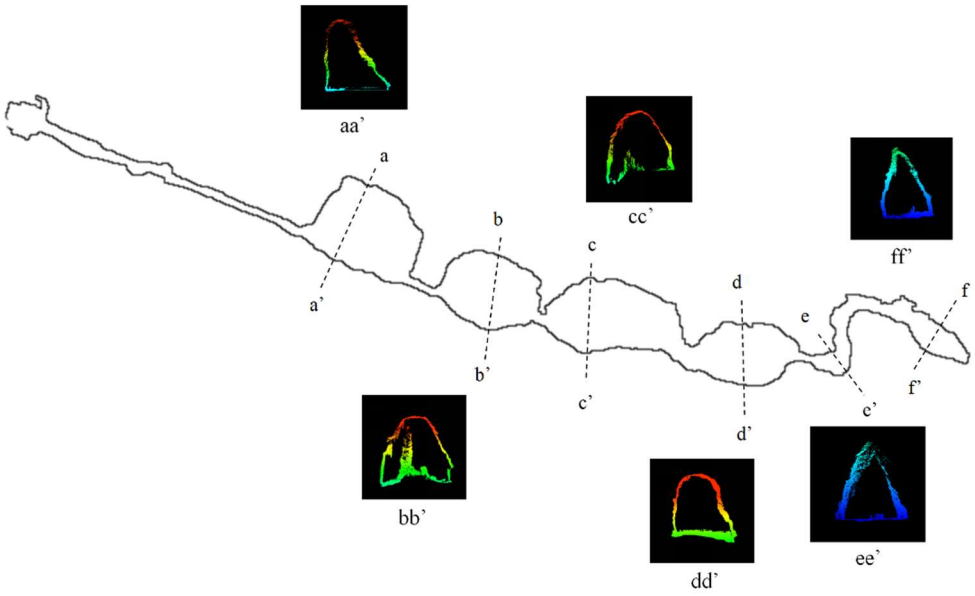

Figure 23. Plane and cross-section map of Yunshui Cave.

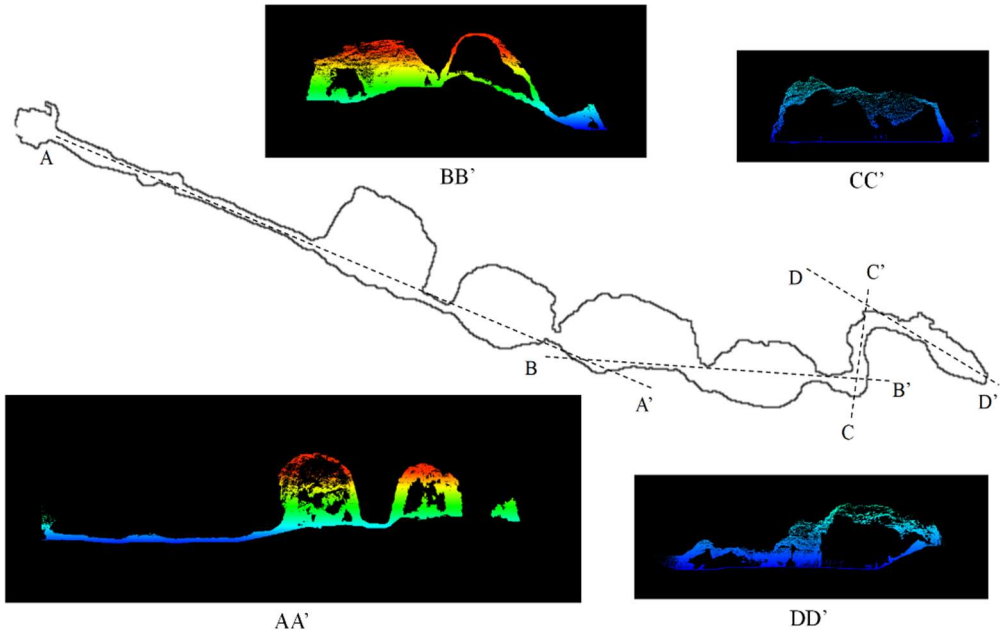

Figure 24. Extension section map of Yunshui Cave.

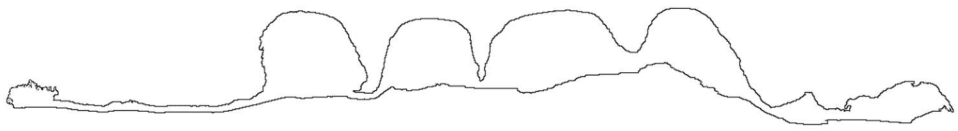

Figure 25. Projection section map of Yunshui Cave in the north–south direction.

At the same time, due to the instability of the karst landform, these images can also be used for safety monitoring and protection. Through observation and measurement of images, possible safety problems can be found and solved in time. After the unstable rock structure is found on the image, it can be supervised in time, and the nearby area can be enclosed to protect the safety of tourists.

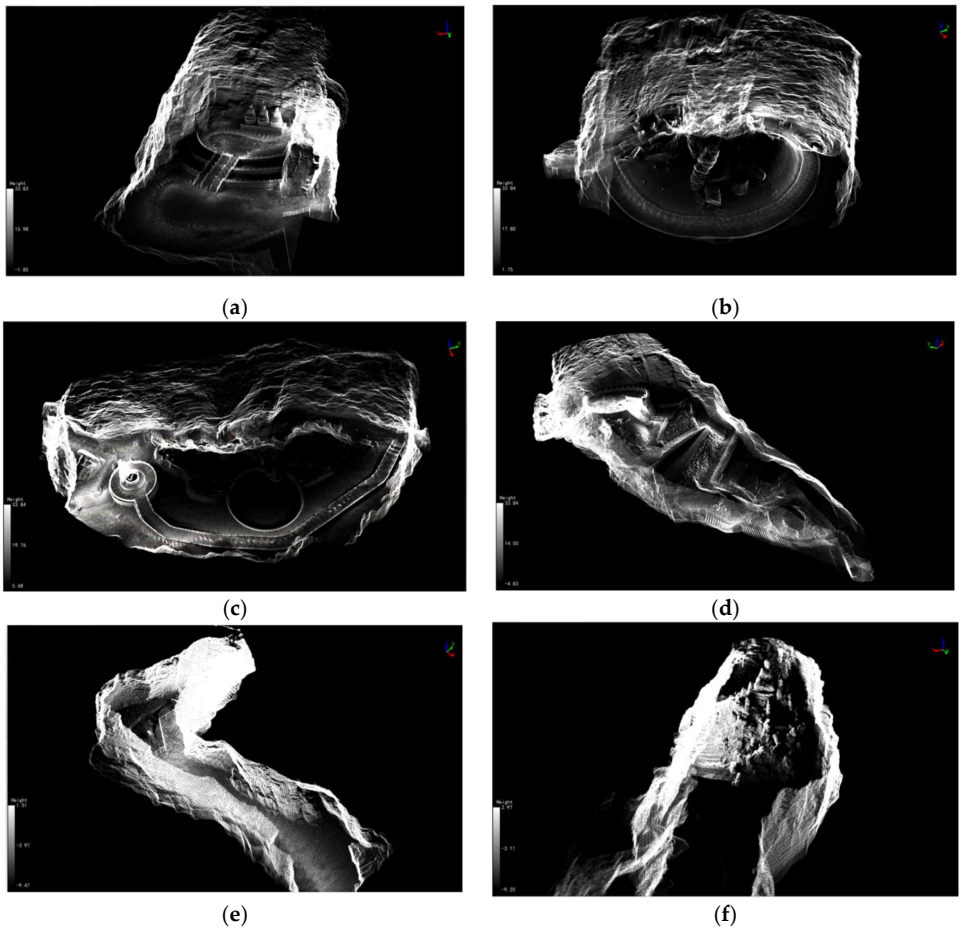

Figure 26. (**a**) The blanking map of Cave 1; (**b**) The blanking map of Cave 2; (**c**) The blanking map of Cave 3; (**d**) The blanking map of Cave 4; (**e**) The blanking map of Cave 5; (**f**) The blanking map of Cave 6.

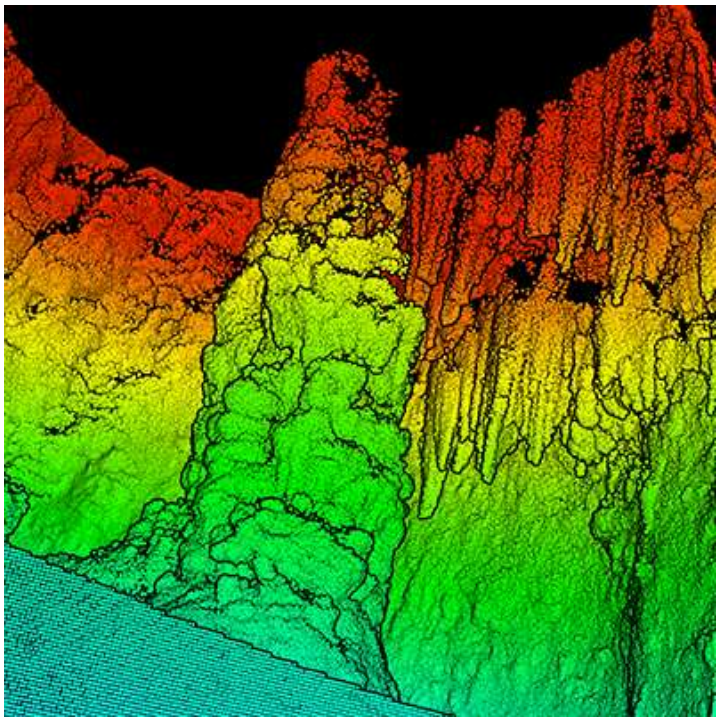

Figure 27. The extracted image of "Sky Pillar" in LiDAR360 V7.2. We can see many details of the stalagmite.

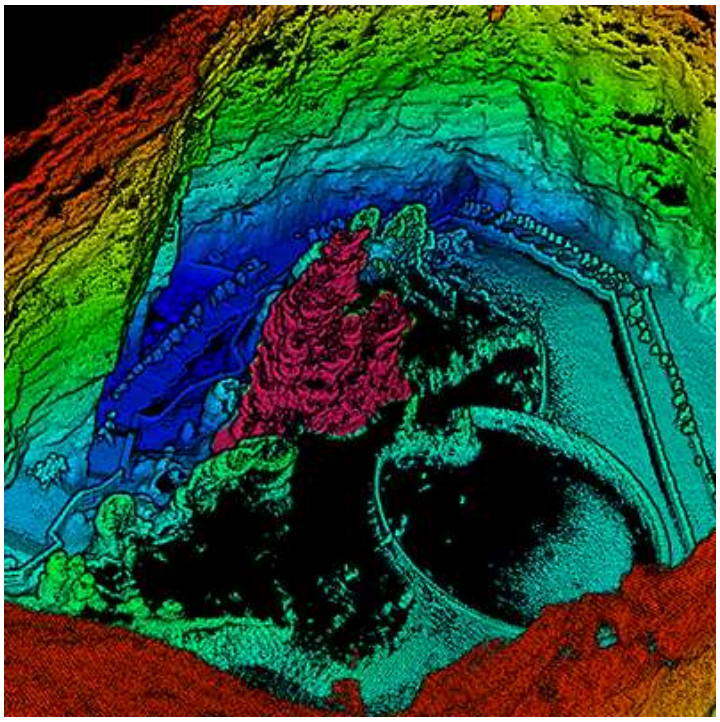

Figure 28. Top view of Cave 3. We can explore various features and details inside the cave.

3.3. GIS Data Analysis

The data obtained by LiDAR technology can be not only imported into LiDAR360 V7.2 but also into GIS software for geographic information analysis. In order to study the terrain and water environment of Yunshui Cave, we extracted the point cloud data at the bottom of the cave and used this data for GIS analysis.

Import the point cloud data of LiDAR into ArcGIS 10.8 and convert it to grid DEM (Digital Elevation Model) data (Figure 29) for further study of Yunshui Cave. The height values on the left side of the figure represent the elevation measurement results based on the entrance of the Yunshui Cave in meters. Positive values indicate being higher than the entrance, while negative values indicate being lower than the entrance. From the DEM data, it can be seen that Cave 4 is the highest, while Cave 5 and Cave 6 are the lowest.

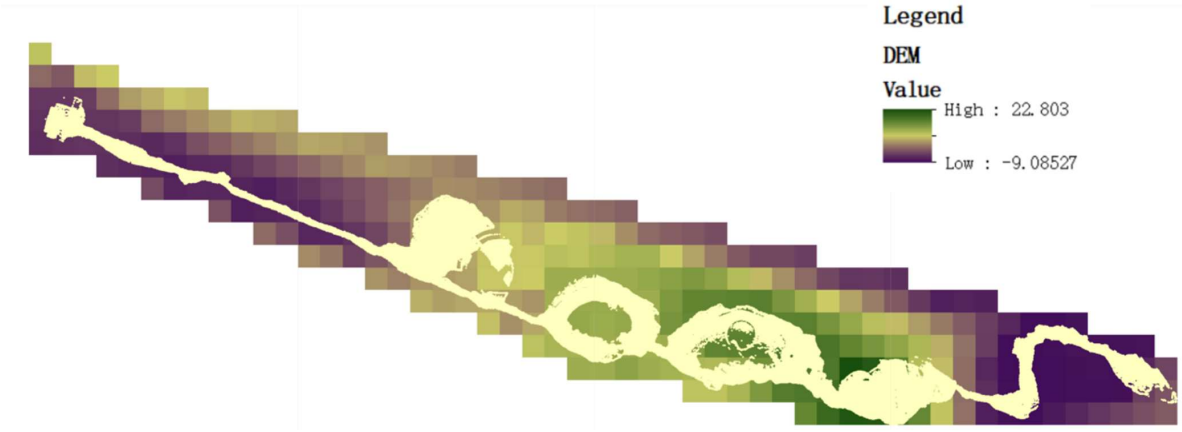

Figure 29. Digital elevation model of Yunshui Cave.

After obtaining the DEM data for Yunshui Cave, the hydrological analysis of Yunshui Cave can be performed in ArcGIS 10.8. We use the Flow Direction tool in ArcGIS 10.8 and the D8 method to create a flow direction grid. The D8 method checks the elevation values of eight adjacent cells around each grid and determines which direction has the lowest

elevation value. The water flows in the direction of this lowest elevation value. The values in various directions, starting from the central grid, are shown in Figure 30. For example, if the steepest descent direction is on the left side of the current processed grid, encoding the flow direction of that processed pixel will be 16.

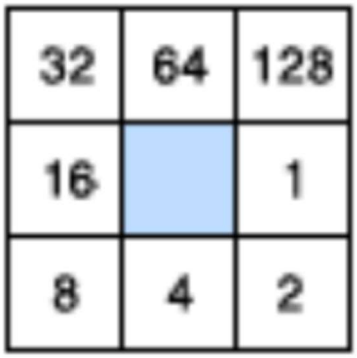

Figure 30. D8 method used in the Flow Direction tool in ArcGIS 10.8. The blue part in the figure represents the grid to be processed.

Figure 31 is the flow direction diagram of Yunshui Cave. According to the flow direction of each area in the cave, if there is water in the cave, it will flow from Cave 3 and Cave 4 to both sides. In fact, Cave 3 and Cave 4 have higher terrain, and the water will flow from the high place under the influence of gravity. The analysis results of the flow direction are consistent with the actual conditions of Yunshui Cave.

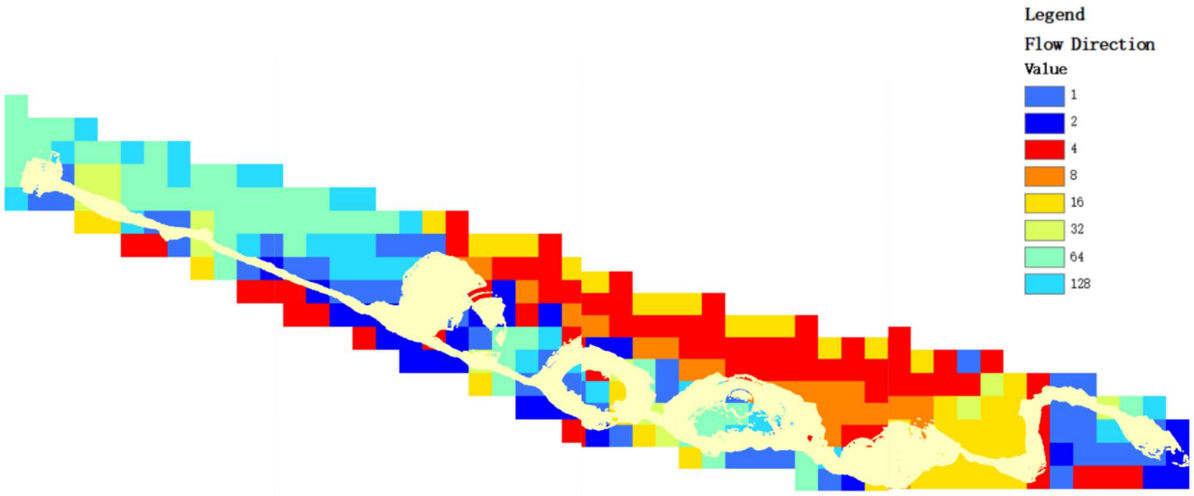

Figure 31. Flow direction diagram of Yunshui Cave.

Figure 32 is the flow accumulation diagram for Yunshui Cave. We use the flow accumulation tool in ArcGIS 10.8. Flow accumulation is used to calculate the cumulative flow, which is the cumulative weight of all pixels flowing into each downhill pixel in the output grid. High-value pixels are concentrated flow areas, while pixels with a value of 0 are local terrain high points.

As can be seen from Figure 32, the flow in the middle section of the entrance corridor and Cave 5 is relatively high. Compared with other caves, Cave 5 has a lower terrain, and the corridor between Cave 4 and Cave 5 has a slope. If there is water in the Yunshui Cave, it is easy to form a large flow here due to the influence of gravity. The entrance corridor was artificially expanded during the development of the scenic area, and the original geological structure was destroyed. The entrance corridor is greatly affected by human activities, which are not regarded as the focus of research. The results of the analysis of the flow rate are consistent with the actual conditions of Yunshui Cave.

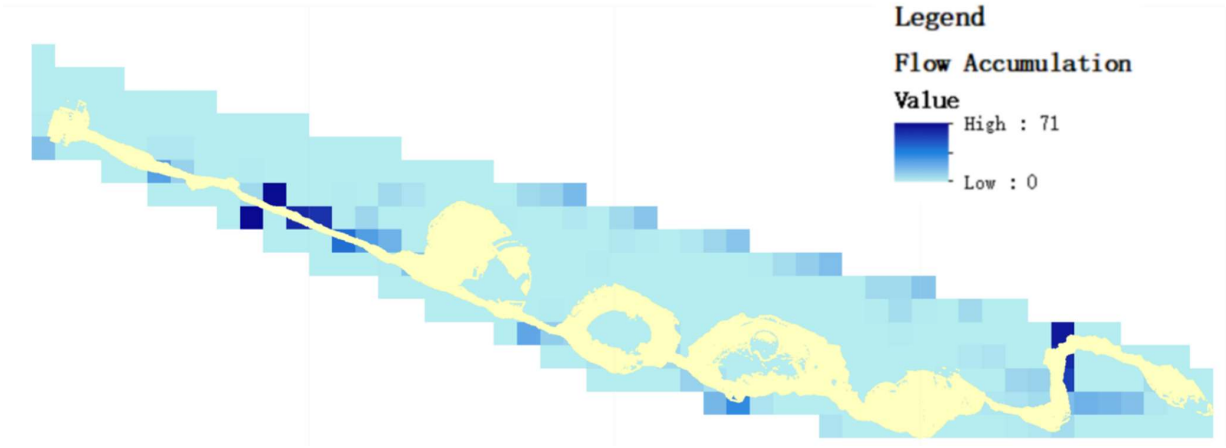

Figure 32. Flow accumulation diagram of Yunshui Cave. The yellow part in the figure represents the point cloud data at the bottom of the Yunshui Cave.

Figure 33 is the watershed diagram of Yunshui Cave. We use the Watershed tool in ArcGIS 10.8 to determine the convergence area above a set of pixels in the grid. The calculation of water needs to combine flow direction results and flow calculation results. The values of each catchment area will be taken from the values of the source in the input grid. The larger the value, the easier it is for this area to collect water. The watershed area is mainly distributed in Cave 5 and Cave 6, which is consistent with the above analysis results of the flow direction and flow rate of Yunshui Cave.

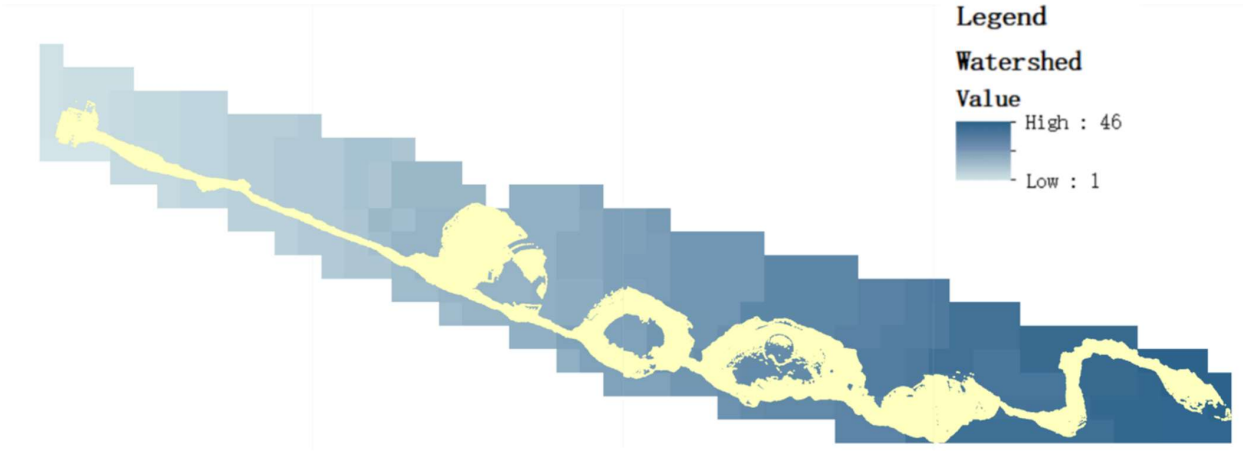

Figure 33. Watershed diagram of Yunshui Cave. The yellow part in the figure represents the point cloud data at the bottom of the Yunshui Cave.

Based on the above analysis of LiDAR images in ArcGIS 10.8, it can be seen that LiDAR technology can not only obtain digital investigation results but also easily bring all the details of field investigation back to the laboratory for real-scene reproduction through modeling and GIS technology. By combining LiDAR technology and GIS technology, the geological structure of Yunshui Cave can be further analyzed, and the analysis results can also be shared and spread through the network.

4. Discussion

4.1. Analysis and Inference Based on Accurate Point Cloud Data from LiDAR

Surface water can erode the rock along the joints of the rock, and it is easier to form large underground caves at the intersection of the cracks. As can be seen from the LiDAR image, the shape of Cave 1 to Cave 4 is similar, and the tops of the caves are basically on the same plane; the volumes of Cave 5 and Cave 6 are significantly smaller compared with

the first four caves, and the height of the top is lower. Therefore, we speculate that the formation time and environment of Cave 5 and Cave 6 are different from the first four caves. The first four caves were formed before Cave 5 and Cave 6. In the development process of underground karst caves, the trend of the bottom of the cave can determine which direction of rock the water dissolves under the influence of gravity. Over the years, the cave will continue to develop in the direction of the trend. Combined with the GIS software analysis of the trend of Cave 4, it can be observed that the slope of the back section of Cave 4 reaches 26° (Figure 22), and the slope direction is consistent with the development direction of Cave 5 and Cave 6. According to this speculation, in the development process of Yunshui Cave, the water in Cave 4 flows down the slope, converges at the bottom of Cave 4, and continues to dissolve the rock to form Cave 5 and Cave 6.

Underground caves often develop underground rivers, and these rivers continue to erode rocks and develop new caves. During the crust movement, the underground river may be truncated, raised, or exposed, altering karst landforms. Accordingly, we infer that there may be a connection between the Yunshui Cave and the Shangfang Mountain Tiankeng. Tiankeng is located in the eastern part of the Yunshui Cave, which may have been a karst cave and may have been connected to the original Yunshui Cave through an underground river. However, crustal movement cut off the original underground river and caused compression deformation, forming the Baidai Peak, where the Yunshui Cave is now located, and the Qinglong Peak, where the Tiankeng is located. Afterwards, the two sets of karst caves developed separately, and the caves at Qinglong Peak collapsed geologically, forming the current Tiankeng. Yunshui Cave and Tiankeng have similar elevations and were formed in similar environments. Most of the other sinkholes were formed in valley areas, except for the Tiankeng, which was formed in the mountains. Therefore, it is highly likely that the karst cave that formed the Tiankeng was originally connected to Yunshui Cave.

In Figure 34, next to the "Sky Pillar" landscape in Cave 2 of Yunshui Cave is another landscape with great research value. These broken stalagmites have been known as "Tower Falling into Three Sections" since ancient times. In LiDAR360 V7.2, we have measured the cross-section of the three parts of the "Tower Falling into Three Sections" (Figure 35). The stalagmite pillar has undergone years of weathering and dissolution, and although the diameters of each section are not exactly the same in the data, they are all around 2.5 m. It can be reassembled into a stalagmite pillar. It is rumored that the original stalagmites were broken due to a major earthquake in the Tang Dynasty and later formed the current landscape. However, the specific formation time remains to be further explored.

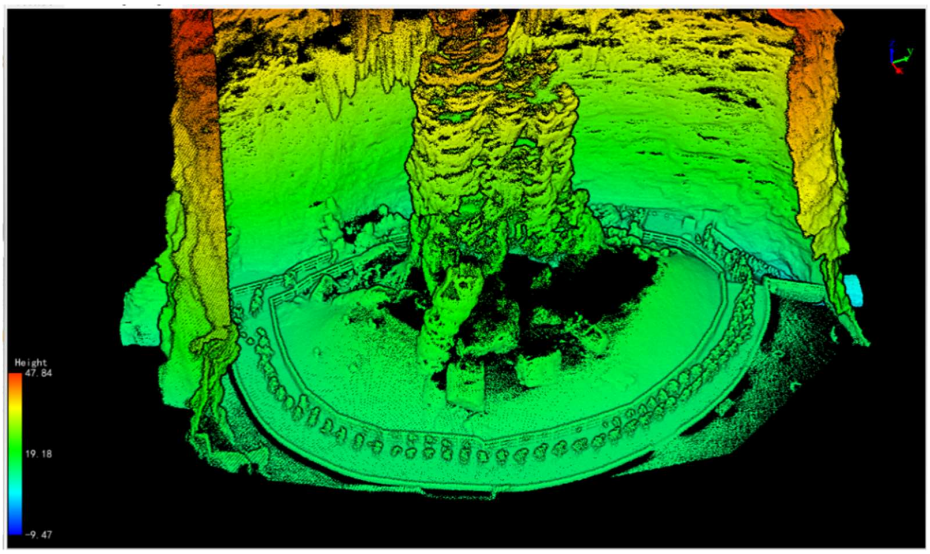

Figure 34. The "Sky Pillar" and the "Tower Falling into Three Sections" landscape in Cave 2.

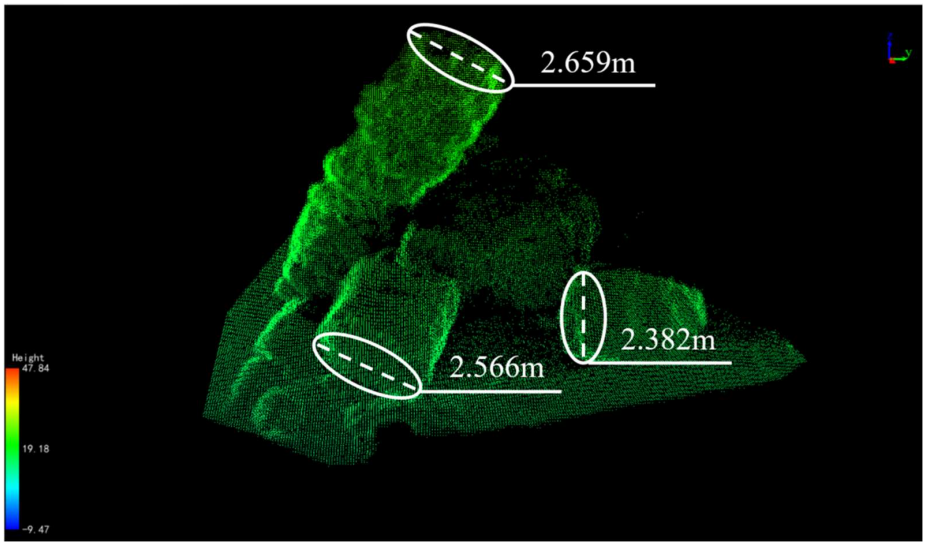

Figure 35. Measurement of landscape and cross-section data for "Tower Falling into Three Sections". Similar diameter data suggests that they may have been a complete stalagmite.

In addition to the seventh cave, which was closed due to its collapse, Yunshui Cave may also have many undiscovered caves. In LiDAR360 V7.2, we can observe that the cave wall of the Yunshui Cave has many bulges, and each bulge may develop a new cave outward. In Figure 36, when observing the top view of Yunshui Cave in LiDAR360 V7.2, we can find that there is a fork in the corridor between Cave 5 and Cave 6, which is the more prominent one in the bulge of the Yunshui Cave wall. In the field investigation, you can also find passages in the fork position, and there seem to be new caves beyond.

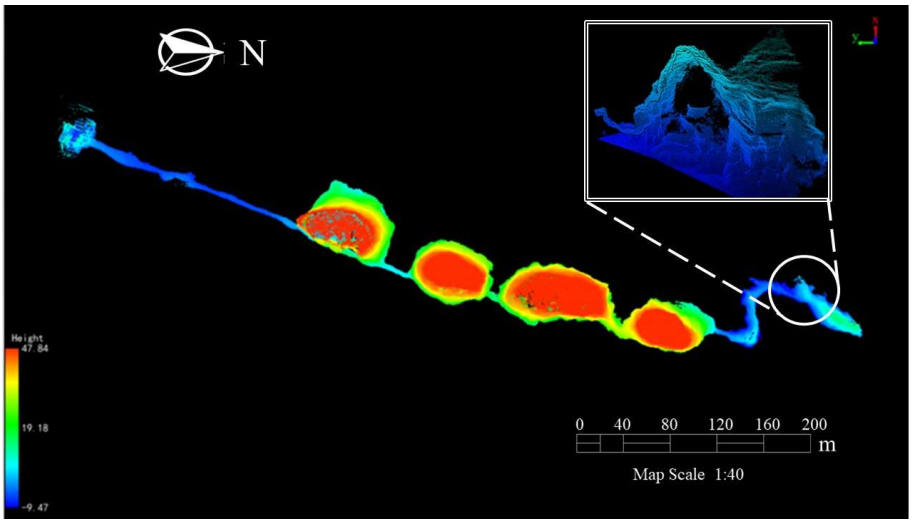

Figure 36. The position of the white circle is the possible location of the new cave.

4.2. The Significance of LiDAR as a New Tool for Geological Surveys

The traditional cave surveying methods, such as the measuring rope used in the previous scientific investigation of Yunshui Cave, have played an immeasurable role in cave exploration and recording. However, LiDAR technology performs excellently in terms of speed, accuracy, and capturing complex cave features, which may be overlooked or inaccurately represented in manual measurements.

As an advanced technology, LiDAR has many advantages in geological investigation. First of all, with its high precision and powerful anti-jamming ability, LiDAR can signif-

icantly reduce measurement error and interference, achieve accurate measurement and identification of the target, and then obtain more accurate data.

Secondly, the LiDAR technology not only provides qualitative information but can also obtain quantitative data, which provides comprehensive information for the research work. Through the scanning and measuring of LiDAR, we can obtain high-precision 3D point cloud data, which is highly visual and can accurately depict the morphology and structure of 3D objects so that users can understand and analyze them more intuitively. In addition, we can also obtain specific numerical data by means of measurement. For example, during the investigation of Yunshui Cave, LiDAR technology helped us obtain accurate three-dimensional topographic data, make high-precision measurements of the cave, and obtain the geometric data of each cave, the geometric data of each scenic spot, and the slope between the caves.

The application of LiDAR technology in the third scientific investigation of Yunshui Cave provides a large amount of accurate basic data and preliminary materials for subsequent geological, environmental, and archaeological investigation and analysis, as well as cultural and tourism resource development. At the same time, it enhances our understanding of the complex geological structure of Yunshui Cave.

In addition, the LiDAR's data are collected in non-contact ways, which means that it is not necessary to directly contact the subject during the acquisition process. This collection method not only avoids possible damage to the measured object but also ensures the safety of the measurement personnel [47]. For example, in the monitoring process of geological disasters, surveyors can scan and monitor at a long distance to ensure their safety. In addition, this non-contact data acquisition method can also simplify the complexity of the collection work and make the data collection more efficient. Compared with traditional methods, LiDAR data can be easily analyzed by using a single computer. This provides a great convenience for the geological investigation.

The application of LiDAR technology in the third scientific investigation of Yunshui Cave provides a large amount of accurate basic data and preliminary materials for subsequent geological, environmental, and archaeological investigation and analysis, as well as cultural and tourism resource development. There are many places in North China with geological environments similar to Yunshui Cave, so we boldly infer that LiDAR technology can be extended to other parts of North China. These areas may include, but are not limited to, karst landforms, mountainous terrain, and areas with complex groundwater systems. Through LiDAR technology, we can efficiently obtain key data such as terrain and topography data, cave structure information, and groundwater flow in other regions, enhance our understanding of other complex underground spatial structures, and provide important support for local geological science research, environmental protection, cultural heritage protection, and tourism resource development.

5. Conclusions

This study is the first time that LiDAR technology has been used to conduct a comprehensive and refined investigation of Yunshui Cave. Its use has allowed us to capture more details than previous studies on Yunshui Cave. Thanks to the development of modern technology, LiDAR cave geological rapid survey technology can go to the precise site that has been chosen for measurement. It also has real-time access to high precision and provides us with hundreds of millions of point cloud data. Compared with the traditional measurement method, the survey efficiency and measurement accuracy are greatly improved. At the same time, it can obtain digital survey results, and through modeling and GIS technology, it can easily bring all the field survey details back to the laboratory for real-scene reproduction. Combining the measurement results with GIS technology, we can not only easily draw the profile of each view of the Yunshui Cave but also obtain slope data that cannot be obtained by traditional measurement methods. Its use gives us the possibility of further analyzing the geological structure, formation processes, and potential risks of the Yunshui Cave through its combination of images and data.

With the aid of LiDAR technology, we were able to rapidly obtain accurate data while also discovering many hidden features of Yunshui Cave. On this basis, we continue to explore the relationship between the six caves or their contacts with each other, which helps us understand the formation process, evolution mechanism, and relationship with the surrounding landscape, such as cave form similarity, etc. In addition, we also found out about many new problems, such as the possible location of new caves, etc., which provide an important reference for future exploration and research.

This study combines the use of LiDAR and geological survey, which is a new model for field geological survey. Referring to this new model, we can also continue to explore other karst landforms in the Shangfang Mountains. We will investigate the further relationship between the Shangfang Mountain Tiankeng and Yunshui Cave, or expand the scope of our research to explore the connection between the karst landform in the Zhoukoudian area and the karst landform in the Shangfang Mountain area; even extending the research scope to North China, studying other places with geological environments similar to Yunshui Cave, obtaining accurate data, and enhancing our understanding of its complex underground spatial structure. This new model not only improves the efficiency and accuracy of geological investigation but also provides a new means for the monitoring of geological disasters. It will help us create a more efficient early warning system. LiDAR technology can provide important support for geological development in multiple regions.

The application of LiDAR technology has solved many problems in traditional measurement methods and led to the promotion of digital geological exploration work. In the future, LiDAR technology will be more widely used in the field of geology, helping the development of geological research in a digital direction. It has important scientific significance and application value.

Author Contributions: Conceptualization, G.A.; methodology, A.S.; software, X.L., A.S. and Y.S.; validation, X.L., A.S. and Y.S.; formal analysis, X.L. and Y.S.; resources, G.A. and Z.D.; data curation, X.L. and Y.S.; writing—original draft preparation, X.L., Y.S., A.S. and N.L.; writing—review and editing, G.A. and X.L.; visualization, X.L. and N.L.; supervision, G.A.; project administration, G.A. and X.L. All authors have read and agreed to the published version of the manuscript.

Funding: This research received no external funding.

Data Availability Statement: The original contributions presented in the study are included in the article, further inquiries can be directed to the corresponding author.

Conflicts of Interest: The authors declare no conflicts of interest.

References

1. Nováková, M.; Gallay, M.; Šupinský, J.; Ferré, E.; Asti, R.; Blanquat, M.d.S.; Bajolet, F.; Sorriaux, P. Correcting laser scanning intensity recorded in a cave environment for high-resolution lithological mapping: A case study of the Gouffre Georges, France. *Remote Sens. Environ.* **2022**, *280*, 113210. [CrossRef]
2. Lee, T.O. An Examination of Close-Range Photogrammetry and Traditional Cave Survey Methods for Terrestrial and Underwater Caves for 3-Dimensional Mapping. Ph.D. Thesis, University of Southern California, Los Angeles, CA, USA, 2018.
3. An, S.; Yuan, L.; Xu, Y.; Wang, X.; Zhou, D. Ground subsidence monitoring in based on UAV-LiDAR technology: A case study of a mine in the Ordos, China. *Geomech. Geophys. Geo-Energy Geo-Resour.* **2024**, *10*, 1–15. [CrossRef]
4. Alhmiedat, T.; Marei, A.M.; Albelwi, S.; Bushnag, A.; Messoudi, W.; Elfaki, A.O. A Systematic Approach for Exploring Underground Environment Using LiDAR-Based System. *CMES-Comput. Model. Eng. Sci.* **2023**, *136*, 2321. [CrossRef]
5. Casana, J.; Laugier, E.J.; Hill, A.C.; Reese, K.M.; Ferwerda, C.; McCoy, M.D.; Ladefoged, T. Exploring archaeological landscapes using drone-acquired lidar: Case studies from Hawaii, Colorado, and New Hampshire, USA. *J. Archaeol. Sci. Rep.* **2021**, *39* (Suppl. C), 103133. [CrossRef]
6. Caspari, G. The Potential of New LiDAR Datasets for Archaeology in Switzerland. *Remote Sens.* **2023**, *15*, 1569. [CrossRef]
7. Wang, Y.; Wang, Z.; Ji, Y. Research on Geological Hazard Risk Assessment in Beijing. *J. Cap. Norm. Univ. (Nat. Sci. Ed.)* **2022**, *43*, 54–61. [CrossRef]
8. Hao, Z.; Yang, Y.; Yun, G.; Liang, Z. Geological landscape and genesis of karst caves in Shangfang Mountain Yunju Temple. *Editor. Dep. J. Geol. Chin. Geol. Soc.* **2005**, *12*, 281–290.
9. Liu, K.; Sun, W.; Wang, S.; Sun, Y. Study on the characteristics of karst development in Beijing. *Carbonates Evaporites* **2020**, *35*, 54. [CrossRef]

10. Li, W.; Wei, Y.; Shi, W. Why is Guilin's landscape unparalleled in the world. *China Min.* **2021**, *30*, 486–488.
11. Ullman, M.; Laugomer, B.; Shicht, I.; Langford, B.; Ya'Aran, S.; Wachtel, I.; Frumkin, A.; Davidovich, U. Formation processes and spatial patterning in a late prehistoric complex cave in northern Israel informed by SLAM-based LiDAR. *J. Archaeol. Sci. Rep.* **2023**, *47*, 103745. [CrossRef]
12. Ye, J.; Wang, G.; Qu, Y.; Cheng, Y. Measured description of Shanyunshui Cave above Beijing. *J. China Univ. Geosci. (Chin. Ed.)* **1982**, *1*, 95–103.
13. Tang, S. Wonderland resort Shangfang Mountain. *BJ Work* **1998**, *5*, 38.
14. Luo, Z. Liao Dynasty Cliff Buddha Statues in Yunshui Cave. *Voice Dharma* **1991**, *9*, 30–31. Available online: https://www.nssd.cn/1dd566f1-2f9d-46a4-918f-40ffb348d042 (accessed on 17 June 2024).
15. Huang, W.; Hou, L. Vertebrate fossils from Yunshui Cave in Beijing. *Vertebr. Hum.* **1984**, *2*, 117–122. [CrossRef]
16. Trimmis, K.P. Paperless mapping and cave archaeology: A review on the application of DistoX survey method in archaeological cave sites. *J. Archaeol. Sci. Rep.* **2018**, *18*, 399–407. [CrossRef]
17. Simek, J.F.; Alvarez, S.; Cressler, A. Discovering ancient cave art using 3D photogrammetry: Pre-contact Native American mud glyphs from 19th Unnamed Cave, Alabama. *Antiquity* **2022**, *96*, 662–678. [CrossRef]
18. Pukanská, K.; Bartoš, K.; Bella, P.; Gašinec, J.; Blistan, P.; Kovanič, Ľ. Surveying and High-Resolution Topography of the Ochtiná Aragonite Cave Based on TLS and Digital Photogrammetry. *Appl. Sci.* **2020**, *10*, 4633. [CrossRef]
19. De Waele, J.; Fabbri, S.; Santagata, T.; Chiarini, V.; Columbu, A.; Pisani, L. Geomorphological and speleogenetical observations using terrestrial laser scanning and 3D photogrammetry in a gypsum cave (Emilia Romagna, N. Italy). *Geomorphology* **2018**, *319*, 47–61. [CrossRef]
20. Beres, M.; Luetscher, M.; Olivier, R. Integration of ground-penetrating radar and microgravimetric methods to map shallow caves. *J. Appl. Geophys.* **2001**, *46*, 249–262. [CrossRef]
21. Di Giacomo, G.; De Giorgi, L.; Ditaranto, I.; Leucci, G.; Miccoli, I.; Scardozzi, G. The Medieval cave village of Casalrotto (Mottola, Apulia): New data on the settlement and its necropolis from archaeological and geophysical measurements. *Measurement* **2018**, *128*, 96–103. [CrossRef]
22. Fedin, K.V.; Kolesnikov, Y.I.; Ngomayezwe, L. Mapping of underground cavities by the passive seismic standing waves method: The case study of Barsukovskaya cave (Novosibirsk region, Russia). *Geophys. Prospect.* **2021**, *69*, 167–179. [CrossRef]
23. Gerovasileiou, V.; Trygonis, V.; Sini, M.; Koutsoubas, D.; Voultsiadou, E. Three-dimensional mapping of marine caves using a handheld echosounder. *Mar. Ecol. Prog. Ser.* **2013**, *486*, 13–22. [CrossRef]
24. Bogue, R. The growing importance of lidar technology. *Ind. Robot Int. J. Robot. Res. Appl.* **2022**, *49*, 1025–1031. [CrossRef]
25. Hammerle, M.; Hofle, B.; Fuchs, J.; Schroder-Ritzrau, A.; Vollweiler, N.; Frank, N. Comparison of Kinect and Terrestrial LiDAR Capturing Natural Karst Cave 3-D Objects. *IEEE Geosci. Remote Sens. Lett.* **2014**, *11*, 1896–1900. [CrossRef]
26. Moreno-Gómez, M.; Liedl, R.; Stefan, C. A New GIS-Based Model for Karst Dolines Mapping Using LiDAR; Application of a Multidepth Threshold Approach in the Yucatan Karst, Mexico. *Remote Sens.* **2019**, *11*, 1147. [CrossRef]
27. Gu, X. Application research of unmanned aerial vehicle airborne LiDAR in geological surveying and engineering surveying. *Appl. Laser* **2020**, *40*, 1126–1131. [CrossRef]
28. Xu, G.; Guo, Q.; Pang, S.; Xue, B.; Tao, S.; Li, W.; Wu, F.; Li, L.; Chen, L.; Li, Y.; et al. Perspectives and prospects of LiDAR in forest ecosystem monitoring and modeling. *Chin. Sci. Bull.* **2014**, *59*, 459–478. [CrossRef]
29. Liang, W.; Wei, Y.; Bai, J.; Wu, M. Application of Unmanned Aerial Lidar in Geological Environment Survey. *Geomat. Spat. Inf. Technol.* **2018**, *41*, 73–75.
30. Šupinský, J.; Kaňuk, J.; Nováková, M.; Hochmuth, Z. LiDAR point clouds processing for large-scale cave mapping: A case study of the Majko dome in the Domica cave. *J. Maps* **2022**, *18*, 268–275. [CrossRef]
31. Kagohara, K. Digital mapping of the natural caves using mobile LiDAR: Example of the Akiyoshi and Taisho Caves. *Bull. Yamaguchi Sci. Res. Cent.* **2023**, *3*, 37–44.
32. Silva, O.L.; Bezerra, F.H.; Maia, R.P.; Cazarin, C.L. Karst landforms revealed at various scales using LiDAR and UAV in semi-arid Brazil: Consideration on karstification processes and methodological constraints. *Geomorphology* **2017**, *295*, 611–630. [CrossRef]
33. Furtado, C.P.Q.; Borges, S.V.F.; Bezerra, F.H.R.; de Castro, D.L.; Maia, R.P.; Teixeira, W.L.E.; Souza, A.M.; Auler, A.S.; Lima-Filho, F.P. The fracture-controlled carbonate Brejões Karst System mapped with UAV, LiDAR, and electroresistivity in the Irecê Basin—Brazil. *J. S. Am. Earth Sci.* **2022**, *119* (Suppl. C), 103986. [CrossRef]
34. Bedford, M.D.; Hrovat, A.; Kennedy, G.; Javornik, T.; Foster, P. Modeling Microwave Propagation in Natural Caves Using LiDAR and Ray Tracing. *IEEE Trans. Antennas Propag.* **2020**, *68*, 3878–3888. [CrossRef]
35. Guo, C.; Xu, Q.; Dong, X.; Liu, X.; She, J. Research on Airborne LiDAR Identification of Geological Hazards in Complex Mountainous Areas. *Geomat. Inf. Sci. Wuhan Univ.* **2021**, *46*, 1538–1547. [CrossRef]
36. Zheng, J.; Shen, A.; Qiao, Z.; Chang, C. 3D digital outcrop based on LiDAR technology and its application in geological modeling: A case study of the Dabantage profile reef beach complex in the Bachu area. *Mar. Orig. Pet. Geol.* **2014**, *19*, 72–78. [CrossRef]
37. Zalevsky, Z.; Buller, G.S.; Chen, T.; Cohen, M.; Barton-Grimley, R. Light detection and ranging (lidar): Introduction. *J. Opt. Soc. Am. A* **2021**, *38*, LID1–LID2. [CrossRef] [PubMed]
38. Yang, W. Research on 3D Laser Scanning Disease Detection Technology for Underground Tunnels. Master's Thesis, Southwest Jiaotong University, Chengdu, China, 2021. [CrossRef]

39. Rao, J.; Yang, T.; Tian, X.; Liu, W.; Wang, X.; Qian, H.; Shen, Z. Vertical structural characteristics of a semi-humid evergreen broad-leaved forest and common tree species based on a portable backpack LiDAR. *Biodivers. Sci.* **2023**, *31*, 23216. [CrossRef]
40. Liu, C.; Yang, W. Collection and spatial modeling of structures using 3D laser scanning. *Geotech. Investig. Surv.* **2006**, *4*, 49–53.
41. Yu, H.; Li, D.; Gao, W.; Wang, S.; Wang, Y.; Ge, S. Analysis of the current situation of tunnel detection based on ground penetrating radar and laser scanning. *J. Changsha Univ. Sci. Technol. Nat. Sci.* **2023**, *20*, 102–117. [CrossRef]
42. Niu, Y. Research on Rapid Identification Method of Dangerous Rock Body Based on 3D Laser Scanning. Master's Thesis, Chengdu University of Technology, Chengdu, China, 2020. [CrossRef]
43. Qiu, T. Research on the Extraction Method of Tunnel Surrounding Rock Information Based on 3D Laser Scanning. Master's Thesis, Chongqing Jiaotong University, Chongqing, China, 2023.
44. Song, Y.; Wang, Z. Using 3D laser scanning technology for quality control and disease detection in subway tunnel construction. *Bull. Surv. Mapp.* **2020**, *5*, 150–154. [CrossRef]
45. Kazhdan, M.; Bolitho, M.; Hoppe, H. Poisson surface reconstruction. *Proc. Fourth Eurographics Symp. Geom. Process.* **2006**, *7*, 61–70.
46. Wang, Z. Research on 3D Human Body Measurement for HoloLens2 Scanning Data. Master's Thesis, Xi'an University of Technology, Xi'an, China, 2023.
47. Farahani, B.V.; Barros, F.; Sousa, P.J.; Cacciari, P.P.; Tavares, P.J.; Futai, M.M.; Moreira, P. A coupled 3D laser scanning and digital image correlation system for geometry acquisition and deformation monitoring of a railway tunnel. *Tunn. Undergr. Space Technol.* **2019**, *91*, 102995. [CrossRef]